AFRL-RV-PS-
TR-2014-0200

REFINEMENT OF REGIONAL DISTANCE SEISMIC MOMENT TENSOR AND UNCERTAINTY ANALYSIS FOR SOURCE-TYPE IDENTIFICATION

Douglas Dreger, et al.

University of California, Berkeley
215 McCone Hall
University of California
Berkeley, CA 94720

2 September 2014

Final Report

AIR FORCE RESEARCH LABORATORY
Space Vehicles Directorate
3550 Aberdeen Ave SE
AIR FORCE MATERIEL COMMAND
KIRTLAND AIR FORCE BASE, NM 87117-5776

DTIC COPY

NOTICE AND SIGNATURE PAGE

Using Government drawings, specifications, or other data included in this document for any purpose other than Government procurement does not in any way obligate the U.S. Government. The fact that the Government formulated or supplied the drawings, specifications, or other data does not license the holder or any other person or corporation; or convey any rights or permission to manufacture, use, or sell any patented invention that may relate to them.

This report was cleared for public release by the 377 ABW Public Affairs Office and is available to the general public, including foreign nationals. Copies may be obtained from the Defense Technical Information Center (DTIC) (http://www.dtic.mil).

AFRL-RV-PS-TR-2014-0200 HAS BEEN REVIEWED AND IS APPROVED FOR PUBLICATION IN ACCORDANCE WITH ASSIGNED DISTRIBUTION STATEMENT.

//SIGNED//	//SIGNED//
Robert Raistrick	Glenn M. Vaughan, Colonel, USAF
Project Manager, AFRL/RVBYE	Chief, Battlespace Environment Division

This report is published in the interest of scientific and technical information exchange, and its publication does not constitute the Government's approval or disapproval of its ideas or findings.

REPORT DOCUMENTATION PAGE

Form Approved
OMB No. 0704-0188

1. REPORT DATE *(DD-MM-YYYY)*	**2. REPORT TYPE**	**3. DATES COVERED** *(From - To)*
02-09-2014	Final Report	09 Sep 2010 – 07 Jun 2014

4. TITLE AND SUBTITLE
Refinement of Regional Distance Seismic Moment Tensor and Uncertainty Analysis for Source-Type Identification

5a. CONTRACT NUMBER
FA9453-10-C-0263

5b. GRANT NUMBER

5c. PROGRAM ELEMENT NUMBER
62601F

6. AUTHOR(S)
Douglas Dreger, Andrea Chiang, Avinash Nayak, Sean Ford, and William Walter

5d. PROJECT NUMBER
1010

5e. TASK NUMBER
PPM00005512

5f. WORK UNIT NUMBER
EF004201

7. PERFORMING ORGANIZATION NAME(S) AND ADDRESS(ES)
University of California, Berkeley
215 McCone Hall
University of California
Berkeley, CA 94720

8. PERFORMING ORGANIZATION REPORT NUMBER

9. SPONSORING / MONITORING AGENCY NAME(S) AND ADDRESS(ES)
Air Force Research Laboratory
Space Vehicles Directorate
3550 Aberdeen Avenue SE
Kirtland AFB, NM 87117-5776

10. SPONSOR/MONITOR'S ACRONYM(S)
AFRL/RVBYE

11. SPONSOR/MONITOR'S REPORT NUMBER(S)
AFRL-RV-PS-TR-2014-0200

12. DISTRIBUTION / AVAILABILITY STATEMENT
Approved for public release; distribution is unlimited. (377ABW-2014-1033 dtd 13 Jan 2015)

13. SUPPLEMENTARY NOTES

14. ABSTRACT

In this study we investigate the inversion of long period regional waveforms for moment tensors with particular emphasis on aspects important for monitoring. We begin with moment tensor inversions for the September 14, 1988 US-Soviet Joint Verification Experiment (JVE) nuclear test at the Semipalatinsk test site in Eastern Kazakhstan, and several nuclear explosions conducted less than ten years later at the Chinese Lop Nor test site. The events are very sparsely recorded with only several stations located within 1600 km. We have utilized a regional distance seismic waveform method fitting long-period, complete, three-component waveforms jointly with first-motion observations from regional stations and teleseismic arrays for the moment tensor (MT). The combination of long-period waveforms and first-motion observations provides unique discrimination of these sparsely recorded events. We demonstrate through a series of Jackknife tests of station geometry, and sensitivity analyses that the source-type of the explosions is well constrained. One event, a 1996 Lop Nor shaft explosion displaces large Love waves and reversed Rayleigh waves at one station indicative of a large F-factor due to tectonic release. We show that in this case the combination of long-period waveforms and P-wave first motions discriminate the event source-type. We further demonstrate the sensitivity of network sensitivity solutions to models of tectonic release and tensile damage over a range of F-factor and K-factor, and investigate the free-surface vanishing traction effect in MT estimation. The results demonstrate a robust source type discrimination capability using seismic moment tensor inversion of long-period, regional distance, complete waveforms under sparse recording conditions. We also present an application of a continuous scanning method to small events recorded locally. The events are associated with the evolution of a sinkhole, but the methods scale and have potential monitoring value. Finally, we demonstrated a statistically based discrimination metric that utilizes the complement of the P-value for earthquake sources and the P-value for NTS nuclear explosions and applied it to the India, JVE, Lop Nor and DPRK nuclear tests. All events cleanly discriminated except for India and the 1996 Lop Nor tests, which were nonetheless identified as being outside of the distribution of naturally occurring earthquakes.

15. SUBJECT TERMS
Seismic moment tensor, regional seismic waveforms, Rayleigh waves, Love Waves

16. SECURITY CLASSIFICATION OF:			**17. LIMITATION OF ABSTRACT**	**18. NUMBER OF PAGES**	**19a. NAME OF RESPONSIBLE PERSON**
a. REPORT	**b. ABSTRACT**	**c. THIS PAGE**			Robert Raistrick
Unclassified	Unclassified	Unclassified	Unlimited	74	**19b. TELEPHONE NUMBER** *(include area code)*

Standard Form 298 (Rev. 8-98)
Prescribed by ANSI Std. Z39.18

This page is intentionally left blank.

Table of Contents

List of Figures

List of Tables

Acknowledgments

We thank Bruce Julian for scripts to make the source-type plots, and Václav Vavryčuk for MatLab code to plot full moment tensors and compare first motions. We thank Weston Geophysical for providing the Humming Albatross waveform data. Plots were made with GMT (Wessel and Smith, 1998).

1. SUMMARY

In this project (FA9453-10-C-0263) we build on our earlier results (DE-FC52-06NA27324, Dreger et al., 2008; Ford et al., 2010; Ford et al., 2009a,b; Ford et al., 2008) to investigate whether source-type populations (explosion, collapse, earthquakes) that were found to separate for the Western US remain separated for other regions of the world. We have expanded our database of studied events to include natural and man-made seismicity from the Korean Peninsula, Kazakhstan, and China. For Kazakhstan and China we have performed waveform modeling to develop calibrated 1D velocity models to improve regional distance moment tensor capabilities in the region, and have refined an approach that combines the use of long-period regional distance waveforms and short-period P-wave first-motions. This combined approach is found to improve discrimination capabilities under very sparse seismic monitoring conditions. In addition, we have compiled source-type distributions for natural seismicity for California for use as a reference in the development of a statistical discrimination approach. We have developed a continuous scanning method that can be applied to targeted regions for autonomous event detection, location, source estimation and discrimination.

2. INTRODUCTION

Ford et al. (2009a) calculated seismic moment tensors for 17 nuclear test explosions, 12 earthquakes, and 3 collapses in the vicinity of the Nevada Test Site in the Western US. They found that the relative amount of isotropic and deviatoric moment provided a good discriminant between the explosions, earthquakes and collapses. Importantly, the populations of explosions and cavity collapses separate dramatically whereas in traditional mb:MS and regional phase P/S ratio discriminants this separation is less clear (e.g. have inconsistent results (Walter et al., 2007)).

In this report we present the analysis of several nuclear and industrial explosions to extend the database of explosion moment tensor solutions. In particular we have developed solutions for the 1988 Joint Verification Experiment event at the Semipalantinsk test site in Kazakhstan, two Chinese tests at the Lop Nor test site that occurred in 1995 and 1996, and an industrial explosion. We have applied a standard seismic moment tensor method (Minson and Dreger, 2008), the network sensitivity solution (NSS) (Ford et al., 2010), and the combination of long-period complete waveforms and P-wave first motions NSS method (Ford et al., 2012), which is described in section 3. The work has resulted in three peer-reviewed publications (Ford et al., 2012; Chiang et al., 2014; Nayak and Dreger, 2014).

3. METHODS, ASSUMPTIONS, AND PROCEDURES

3.1. Event Discrimination using Regional Moment Tensors with Teleseismic-P Constraints

Introduction

The elements of the seismic moment tensor can be used to derive the source type. Determination of the source type and discrimination between explosion, collapse, and earthquake sources can aid in the understanding of deformation in a region and in nuclear explosion monitoring. Ford et al. (2009b) calculated a seismic moment tensor for the announced nuclear test of the Democratic People's Republic of Korea (DPRK) on 25 May (Memorial Day) 2009 using regionally recorded (<1500 km) intermediate period (10–50 s) waveforms. The source type derived from the seismic moment tensor was dominantly explosive. An earthquake source was highly unlikely due to the poor fit to the data for any double-couple (DC), or earthquake-like, source. However, another source type with very little explosive component fit the data almost equally as well as an explosion.

This source is described as a compensated linear-vector dipole (CLVD) with a vertical axis in compression (VCLVD-P). The similarity in data fit between the dominantly VCLVD-P source and dominantly explosive source presents a problem in discrimination between these two source types. The reason for this VCLVD-P–explosion ambiguity is that the regional distance intermediate period recordings of a shallow event are most sensitive to the isotropic tensile radiation pattern along the equator of the focal sphere, which produces Rayleigh waves with uniform source phase, and which does not generate Love waves. The pure explosion and VCLVD-P radiation patterns differ significantly for a small takeoff angle where waves leave the source nearly vertical. The incorporation of additional data sensitive to this vertical region of the focal sphere would constrain the VCLVD-P–explosion tradeoff. We propose to use teleseismic-P recordings to constrain the moment tensor derived source type because the steep takeoff angle of teleseismic-P waves is sensitive to the lower hemisphere of the focal sphere, where they are in dilation for a VCLVD-P and in compression for an explosion.

The use of only teleseismic data to determine the source type has more serious trade-offs in terms of explosion monitoring, where there is little discrimination between shallow reverse mechanism earthquakes, explosions, and VCLVD in tension. However, in the absence of regional data, relative amplitudes of teleseismic body waves offer some ability to determine source type, and this was the approach of Clark and Pearce (1988), Pearce et al. (1988), and Rogers and Pearce (1992). The combined use of regional and teleseismic data to constrain the source type was done qualitatively by Bowers (1997) to discriminate between a collapse, explosion, and an earthquake in a South African mine and by Bowers and Walter (2002) to discriminate between a collapse and an explosion for mine events in Völkershausen, Germany, and Wyoming, United States. In those studies the teleseismic-P waveform was shown to be inconsistent with sources determined via regional waveform fitting. A similar approach is used here, but with a

more quantitative component afforded by the use of a source-type plot (Hudson et al., 1989) with application to the 2009 Memorial Day explosion in the DPRK.

Figure 1 shows the distribution of regional and far-regional distance stations that were used in the analysis, and the global locations of three arrays that were used to obtain P-wave polarities. Seismic moment tensor solutions were obtained using the Network Sensitivity Solution (NSS) method developed by Ford et al. (2010). In Figure 2 the waveforms for several mechanisms sampled in the NSS space are compared. It is notable that while there is essentially the same level of fit between the full moment tensor solution and the deviatoric moment tensor solution there is a marked difference in fit level with double-couple solutions. The NSS source-type space (Figure 2c) shows the theoretical tradeoff between a explosion source and a CLVD with a vertical major vector dipole in compression (a negative CLVD). The NSS represents the best fit surface of a uniform distribution of moment tensor solutions in source-type space. It is important to note that the construction of the NSS involves the forward testing of upwards of 30 million moment tensor solutions, and that there are many mechanisms of different orientations (orientation of eigenvectors, strike/dip/rake, and azimuth and plunge of CLVD major vector dipole).

The three dots in each of the focal mechanisms show the locations of the P-wave observations derived from array analysis at three global distance arrays. The first motions are all up. It is evident that the first motions eliminate some of the double-couple solutions, however the regional long-period waveforms clearly eliminate the possibility of such solutions for this event. The first motions are also seen to be inconsistent with the down first motion region of the deviatoric solution.

Starting with the NSS shown in Figure 2c we tested solutions against the teleseismic first motion observations, where if a particular moment tensor solution violates the first motion observations the goodness of fit parameter for that solution is set to zero. Figure 2d shows the results of this test. The deviatoric line in the source type diagram is eliminated from possible solutions, and the best fitting region is tightly defined around the full moment tensor inversion result. The use of teleseismic first motions eliminates the theoretical tradeoff between pure explosion and negative CLVD sources.

Figure 2c and 2d demonstrate that the incorporation of teleseismic-P information can eliminate the theoretical tradeoff between explosion and –CLVD sources due to similarity in surface wave radiation patterns, and greatly improve the characterization of the explosive nature of the event. This work was published in the Bulletin of the Seismological Society of America (Ford et al., 2012).

In section 3.2 we refine this approach to utilize regional P-wave first motion data, as well as a modified goodness of fit criterion.

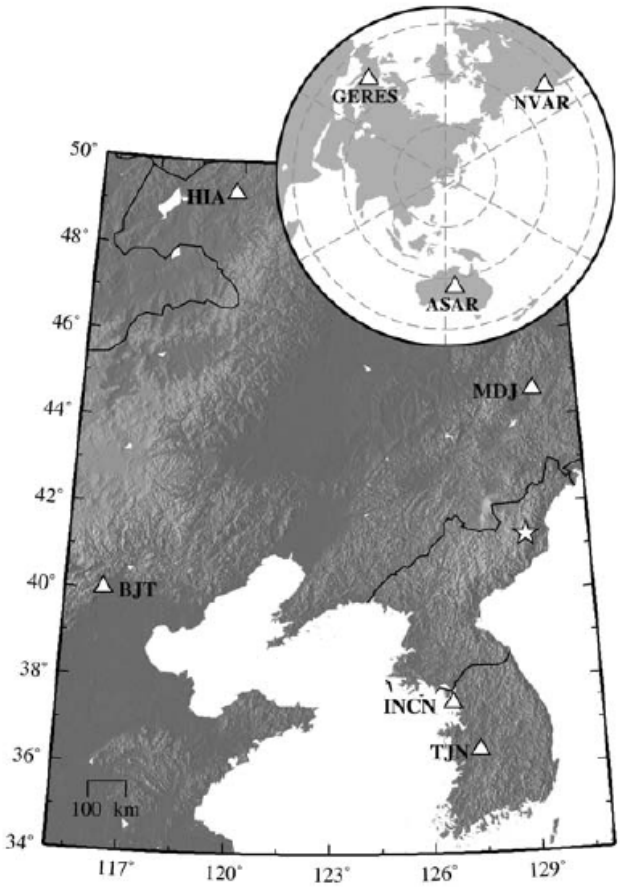

Figure 1. Map of the Yellow Sea and Korean Peninsula with the 2009 Memorial Day explosion (star) and the regional stations used in the analysis (triangles). *Inset: azimuthal equidistant map of teleseismic arrays used in the analysis (triangles), where the origin is the location of the explosion.*

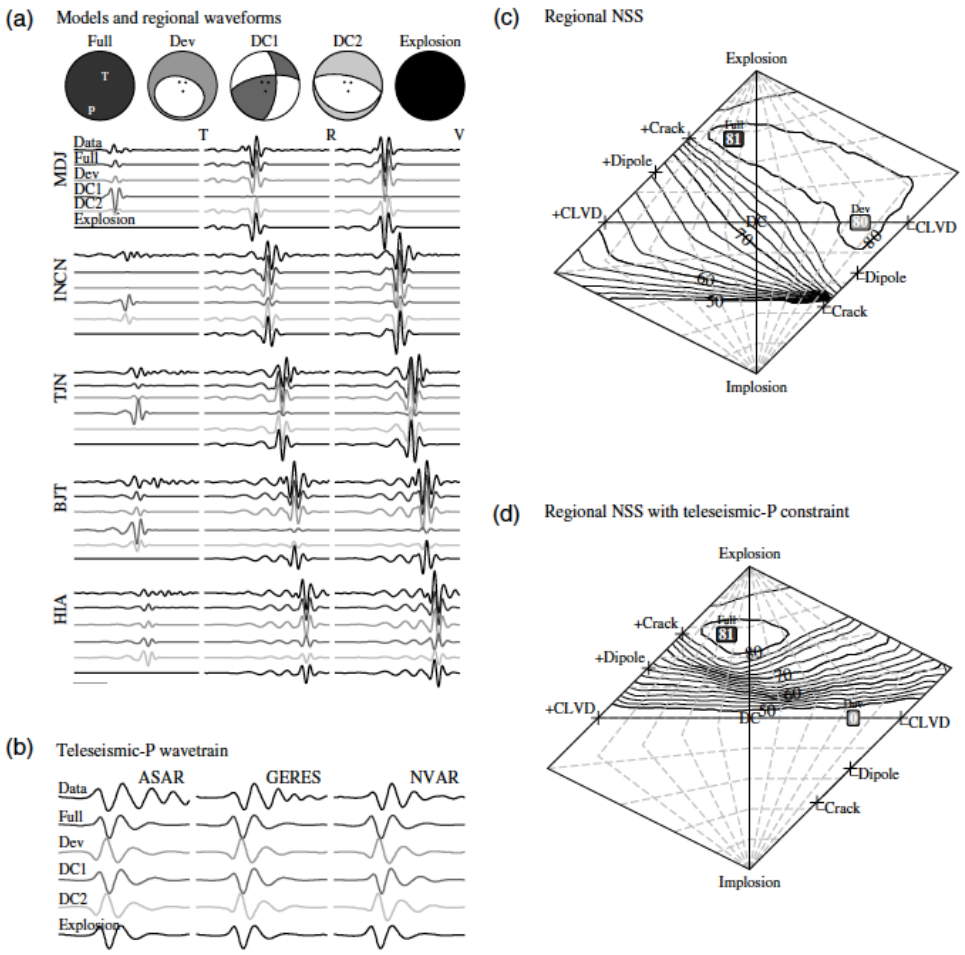

Figure 2. Teleseismic constraint to regional source-type determination. *(a) Three-component (tangential, T; radial, R; and vertical, V) intermediate-period (10-50s) displacements (labeled Data) from regional stations shown in Figure 2 and synthetic waveforms at those stations predicted by the sources shown with a lower-hemisphere equal-area focal sphere. Amplitudes are normalized to the maximum of the three components at each station. The gray bar near the bottom is 50 s long. The gray scale of the compressional component of the focal sphere matches the gray scale of the predicted waveform and is also noted for MDJ waveforms. The T and P axes are plotted on the focal sphere of the best-fit full moment tensor (labled Full). The dots show the teleseismic P-wave polarity (all up) for the three teleseismic arrays. (b) Array beams of high-frequency (0.8 to 4.5 Hz) teleseismic-P wave trains (labeled Data). As in (a) the gray scale relates predicted solutions to specific source types. (c) Contours of fit (variance reduction), VR, equation 1) to the regional data for a uniform distribution of sources on a source-type plot. (d) The NSS shown in (c) where VR is now zero if the teleseismic-P and forward predicted data are uncorrelated, as is the case for the deviatoric source.*

3.2. Analysis of the 1988 Soviet JVE and 1990's Chinese Lop Nor Tests

Introduction

The use of regional distance long-period, complete waveform data to determine the seismic moment tensor and discriminate the source-type of earthquakes, underground cavity collapse and nuclear explosions has been demonstrated for events in the western United States (Dreger *et al.*, 2008; Ford *et al.*, 2008; Ford *et al.*, 2009a), and for the recent 2006 and 2009 North Korean nuclear tests (Ford *et al.*, 2009b; Ford *et al.*, 2010). In these studies populations of earthquakes, underground cavity collapses and nuclear explosions are found to separate when considered on a Hudson *et al.* (1989) source-type diagram. The source type plot simplifies the moment tensor into two parameters that depend on the eigenvalues of the moment tensor. These parameters T and κ describe the deviation from a pure-double-couple in terms of non-volumetric (compensated linear vector dipole, CLVD) and volumetric components. Ford *et al.* (2010) utilized the Hudson *et al.* (1989) source-type representation to develop a network sensitivity solution (NSS), which tests on the order of 100 million moment tensor solutions uniformly distributed in source-type space to determine the best fitting solution, the uncertainty in the solution, and the capabilities of the method given the topology of a recording station network. The regional distance moment tensor inversion, coupled with NSS analysis, and the characterization of sensitivities and uncertainties due to random errors and systematic velocity model errors enable the discrimination of source-type in relatively sparse regional distance monitoring.

We investigate the 14 September 1988 US-Soviet Joint Verification Experiment (JVE) nuclear test at the Semipalatinsk test site in Eastern Kazakhstan, and two nuclear explosions conducted less than ten years later at the Chinese Lop Nor test site (Table 1). These events were very sparsely recorded by stations located within 1600 km, and in each case only 3 or 4 stations were available in the regional distance range (Figure 3a) for moment tensor analysis. Following the results of Ford *et al.* (2009b) we incorporated first-motion data from the regional stations, as well as teleseismic stations to provide additional constraint in the NSS analysis. The results show that unique discrimination of these events is possible under these extremely sparse monitoring conditions when long-period regional waveforms and P-wave first-motion polarities are combined.

Table 1. Event Hypocenter Information

	1988 JVE	1995 Lop Nor	1996 Lop Nor	1999 Lop Nor EQ
Origin Time (UTC)	03:59:57.30	04:06:00.20	02:56:00.06	03:51:05.42
Latitude, longitude	49.882, 78.882	41.553, 88.7496*	41.5804, 88.6893*	41.674, 88.463
Depth (km)	<1.0	0.7*	0.5*	17
Mb†	6.1	6.1	5.9	5.9
M_S‡	4.8	5.0	4.3	5.3
M_W	5.2	5.2-5.4	5.2	5.3
F	0.97 to 1.15	3.79 to 4.20	-12.75 to -20.44	
K	2.59 to 2.73	2.80 to 2.88	2.81 to 2.90	
T	-0.87 to -0.91	-0.82 to -0.83	-0.62 to -0.66	0.1424
κ	0.57 to 0.59	0.56 to 0.57	0.36 to 0.39	0.0540

* Waldhauser et al. (2004)
† Priestly et al. (1990); Yang et al. (2003)
‡ ISC catalog (Explosions); NEIC catalog (Earthquake)

Data Processing and Methods

Data and instrument response for the US-Soviet Joint Verification Experiment (JVE) and Lop Nor nuclear tests were downloaded from the Incorporated Research Institutions for Seismology (IRIS, see Data and Resources section) that consists of a collection of stations from the regional broadband seismic network in China, the Global Seismic Network (GSN), and other temporary networks (Figure 3a). In addition to data from IRIS for the 1988 Soviet JVE, we also have data from temporary deployments of short period instruments located at near-regional distances < 260 km (Priestley *et al.*, 1990) and the Borovoye station (BRVK) at a distance of 690 km. The data was instrument corrected, integrated to displacement, rotated to radial and transverse components, and filtered between 12.5 to 80 seconds with a Butterworth filter depending on instrument type and signal-to-noise levels. Table 2 lists the stations used for each event, and the frequency passband that was employed. The processed data were then inverted using the time domain full waveform moment tensor inversion of Minson and Dreger (2008). For JVE we used a source depth of 1 km that gives the highest goodness of fit between data and synthetics, and for the two Lop Nor events we used the source depths from Waldhauser *et al.* (2004). We then inverted the data with Green's functions computed for a range of source depths to determine the source depth sensitivity.

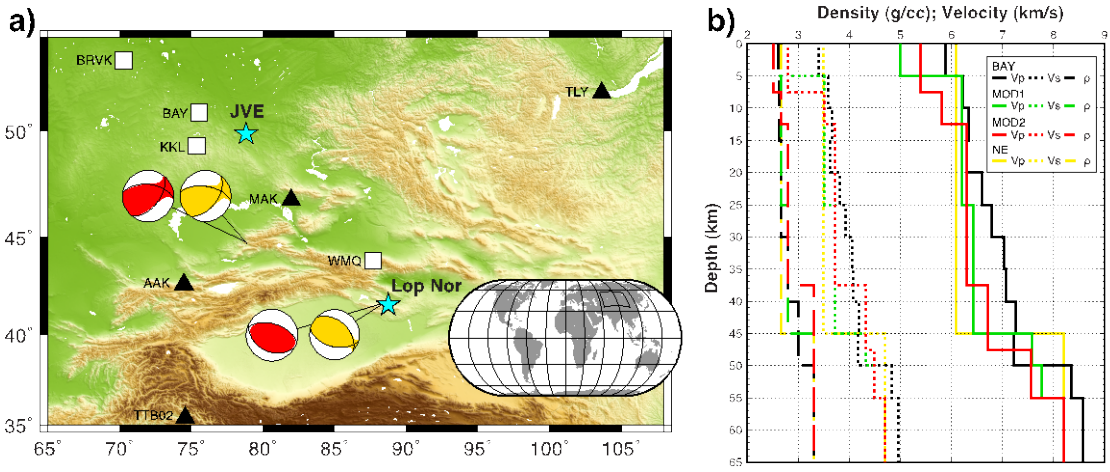

Figure 3. **a)** Event locations (star) and seismic stations (triangle and square) used in the moment tensor analysis. *The two Lop Nor events are located very closely hence the overlapping stars. Triangles represent the stations used in the analysis of the 15 May 1995 Lop Nor explosion, 8 June 1996 Lop Nor explosions, and squares are the stations used in the 14 September 1988 Soviet Joint Verification Experiment. Focal mechanisms of local earthquakes used in the velocity model calibration are also plotted. On the right is the solution from this study and on the left is the Harvard GCMT solution.*
Figure 3. **b)** Velocity models used in the analysis. *BAY from Walter and Ammon (1993); MOD1 from broadband waveform modeling of local earthquakes (Fig. 3a); MOD2 is a 1D model simplified from Sun et al. (2010)'s surface wave tomography; NE is a simple layer over halfspace model.*

The seismic moment tensor consists of nine force couples that represent the equivalent body forces for seismic sources of different geometries (Jost and Herrmann, 1989), that due to conservation of angular momentum reduce to six independent couples and dipoles. The data are represented by the convolution of Green's functions for a given Earth model, source terms and the moment tensor elements. The individual moment tensor elements are obtained using a generalized least square inversion and the goodness of fit between the data and synthetics is measured by the variance reduction (VR) given by:

$$VR = \left(1 - \frac{\sum (d_i - s_i)^2}{\sum d_i^2}\right) \cdot 100 \qquad (1)$$

where d represents the data and s represents the synthetic waveforms.

Because the data are linear combinations of the Green's functions weighted by their associated moment tensor elements, we need a well-calibrated velocity model in order to estimate robust seismic source parameters. For each test site we utilized several published seismic velocity models, and for some paths we additionally calibrated models by modeling earthquake records. The inversion method also allows for small time shifts

between the data and Green's functions to compensate for errors in origin time, location, and in velocity structure.

In addition, we use two alternate methods in order to fully characterize the source solution space. One utilizes a grid search to find the best-fitting double-couple (DC), pure-isotropic/explosion (ISO), or DC + ISO source mechanism. The other, described below, utilizes a moment tensor grid search in order to assess solution uniqueness and resolution of source-type.

Although the seismic moment tensor inversion gives a unique moment tensor solution, the decomposition of the moment tensor solution is non-unique. Therefore we implemented the Hudson *et al.* (1989) source-type representation that circumvents the need to decide on a particular moment tensor decomposition scheme. The source-type diagram has two key parameters T=-2ε and κ on the x- and y-axis, respectively, given by the equations:

$$\varepsilon = \frac{-m_1'}{|m_3'|}, \quad m_3' + m_2' + m_1' = 0, \quad |m_3'| \geq |m_2'| \geq |m_1'| \tag{2}$$

$$\kappa = \frac{M_{iso}}{|M_{iso}| + |m_3'|}, \quad M_{iso} = (m_3 + m_2 + m_1)/3 \tag{3}$$

m'_1 and m'_3 are the deviatoric principal moment associated with the minimum and maximum principal compressive stress axes, and M_{ISO} is the isotropic moment. Equation (2) measures the deviation from a pure shear dislocation and equation (3) describes the volume change. In this convention, ε is 0 for a pure DC source and ±0.5 for a pure CLVD source, and κ is ±1 for a spherical explosion and implosion, respectively. Understanding the relative contributions of the different moment tensor elements provides insights into the complex source processes of explosions as well as other seismic events. This representation of the seismic source has been shown to result in separate populations for explosions, underground cavity collapse and earthquakes (Ford *et al.*, 2009a; Ford *et al.*, 2009b; Dreger *et al.*, 2008; Ford *et al.*, 2008) enabling discrimination capability.

Table 2. Even-Station Combinations & Passbands

Event	Station	Passband (s)	Distance (km)	Azimuth (deg)
1988 JVE	BAY	12.5-20	255	257
	KKL	12.5-20	256	295
	BRVK	12.5-30	690	304
	WMQ	20-50	953	132
1995 Lop Nor	MAK	30-50	796	319
	AAK	30-50	1184	281
	TLY	30-50	1597	40
1996 Lop Nor	MAK	30-50	794	319
	AAK	30-80	1184	280
	TTB02	30-50	1410	246
1999 Lop Nor EQ	WMQ	30-50	246	346
	PDG	30-50	760	287
	MAKZ	30-50	770	320
	TLG	30-50	940	284
	TLY	30-50	1602	41

To assess the confidence of the moment tensor solution, we implemented the Network Sensitivity Solution (NSS) technique developed by Ford *et al*. (2010). The technique presents the level of fit between actual data and the different theoretical solutions described by the source-type diagram for a given station configuration, Earth model, and frequency band. From the NSS of a given event we can determine whether or not the best fitting full moment tensor solution from the inversion is well-resolved to make useful interpretations about the source. We included regional and/or teleseismic P-wave first motions in addition to waveform data in the NSS analysis (Ford *et al.*, 2012) to better constrain the moment tensor solution. To include P-wave polarities as additional constraints, we take the suite of synthetic moment tensor solutions from the previous waveform NSS, compute their P-wave polarities, and compare them to the observed P-wave polarities. We assign -1 for downward motion and +1 for upward motion. The VR is calculated as:

$$VR = \left(1 - \frac{\sum\left(Pol_{obs} - Pol_{synth}\right)^2}{\sum Pol_{obs}^2}\right) \cdot 100 \tag{4}$$

Then we calculate the combined waveform and first motion VR as:

$$VR = \left(sVR_{waveforms} \cdot sVR_{firstmotions}\right) \cdot 100 \tag{5}$$

where sVR_{reg} and sVR_{fm} are normalized by the maximum regional waveform and first motion VR, respectively. The take-off angles are calculated using *iaspei-tau* (Snoke, 2009) and the iasp91 reference Earth model. Incorporating the first motion data proves to be a powerful tool eliminating solution non-uniqueness, and in assessing the confidence

of a solution under sparse station coverage monitoring situations. We find that additional polarity constraints assist by uniquely discriminating the events as predominantly explosive.

This powerful result is due to the fact that the tradeoff between a pure explosion and negative CLVD (Ford *et al.*, 2012) only occurs for a negative CLVD in which the compressional major vector dipole is vertically oriented. For these two sources and combinations of the two, the surface wave radiation patterns are identical for Rayleigh waves, and are theoretically null for Love waves. This vertical CLVD mechanism predicts dilational first motions in the center of the focal sphere. For explosions, the incorporation of P-wave first motion data, particularly teleseismic observations with low takeoff angle proves to be an effective test against the negative CLVD source type. Naturally challenges remain for cases with low signal-to-noise in P-waves, or cases in which free-surface reflections, or interactions with nearby velocity structure result in reversed dilational polarities. Furthermore, the absence of good P-wave polarities from teleseismic arrays or stations may require the use of regional seismic waveform data alone. Nevertheless, as will be shown in the following, even in such regional distance, sparse coverage situations, the combination of low-frequency full waveform fits with regional distance P-wave first-motions, greatly enhances the discriminatory power of the method.

14 September 1988 Soviet Joint Verification Experiment (JVE)

Our analysis of the Soviet JVE event included three stations in Eastern Kazakhstan and one station in northwestern China. Stations BAY and KKL are filtered between 12.5 to 20 seconds, station BRVK is filtered between 12.5 to 30 seconds, and station WMQ is filtered between 20 to 50 seconds. The use of station-specific filters allows tailoring of the approach for path specific signal-to-noise levels, and with respect to the suitability of the velocity model used to compute the Green's functions. We used a well-calibrated velocity model BAY (Walter and Ammon, 1993) for the Eastern Kazakhstan stations and tested two models for the path to the Chinese station WMQ. The two models used for station WMQ are from broadband waveform modeling of two local earthquakes in Kazakhstan and the Lop Nor nuclear test site, called MOD1 (Fig. 3b), and another 1D model simplified from surface wave tomography (Sun *et al.*, 2010), called MOD2. Figure 3b shows all the velocity models used in this paper to calculate the Green's functions and generate the synthetic seismograms. We have both regional P-wave first motions including the four stations used in the waveform inversion (Walter and Patton, 1990; Priestley *et al.*, 1990), and teleseismic P-wave first motions from the Adirondack array in New Hampshire, reported by Battis and Cipar (1991), and Gauribidanur array in India. The best fitting source mechanism from full moment tensor inversion of regional waveforms consists of a predominantly explosive component and a moment magnitude (M_W) between 5.21 and 5.25, depending on the velocity model used. The calculated moment used the convention for total moment described by Bowers and Hudson (1999). M_W falls close to the surface wave magnitude (M_S) in the catalog because the frequency range we used in the inversion is dominated by long period surface waves. Respective VRs for a full, deviatoric, DC, DC+ISO, and ISO mechanism are 84-

85%, 79-80%, 75-76%, 81-82%, and 77-78%. Variations in VR resulted from different velocity models (MOD1 and MOD2) used for WMQ. The goodness of fit between data and synthetics are similar for the five different moment tensor decompositions shown in Figure 4, due to the dominance of surface waves, and presence of Love waves, but a pure DC solution has the poorest VR as compared to the other four decompositions that are either purely isotropic or included an isotropic component.

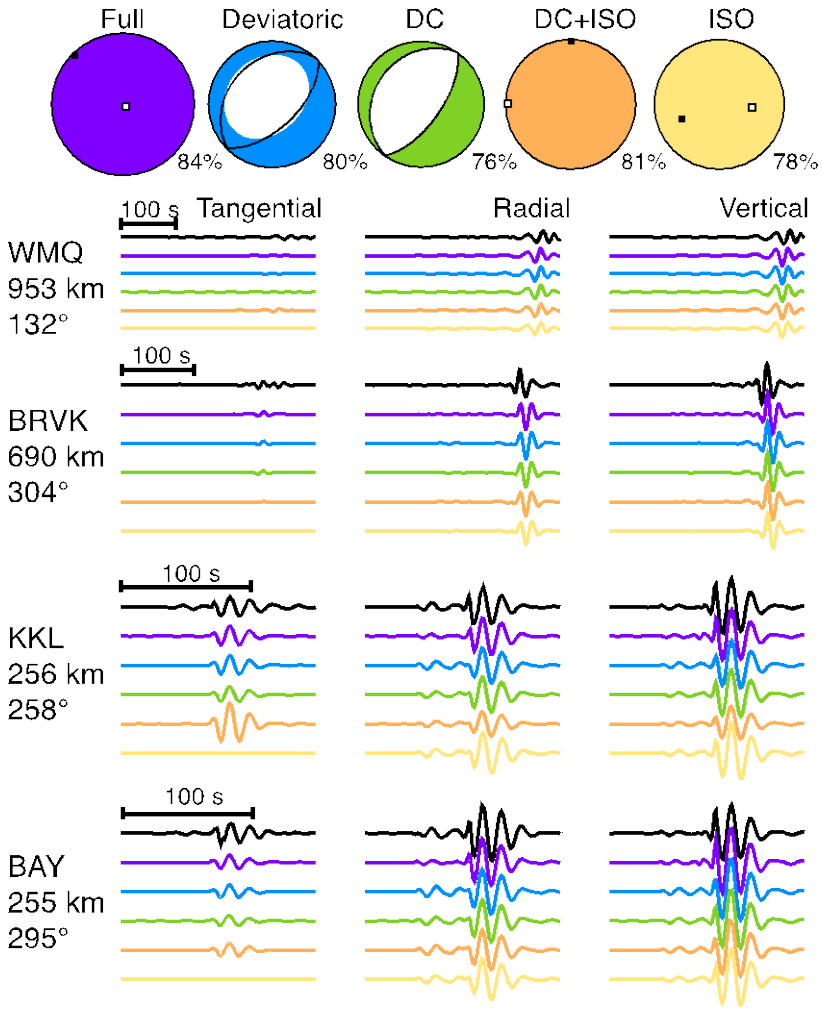

Figure 4. 1988 Soviet JVE Source Model and Waveform Comparisons. *The top trace is the observed waveform data and the rest are synthetic waveforms according to their corresponding source mechanisms (The order from top to bottom is: data, full, deviatoric, double-couple (DC), DC + isotropic (ISO), and ISO). Station name, source-receiver distance, azimuth and maximum amplitude are shown. Associated variance reduction (VR) for each source type is plotted next to their focal mechanisms. Data shows small Love waves on the tangential component, characteristic of an explosion. We show results using Green's functions calculated from MOD2 for WMQ.*

We computed the NSS using three different combinations of data sets: (1) from regional waveforms, (2) combined waveform, regional and teleseismic P-wave first

motions, and (3) combined waveform and four regional P-wave first motions. We also compare the NSS using different Earth models MOD1 (Fig. 5a-c) and MOD1+MOD2 (Fig. 5d-e) to compute the Green's functions. The regional waveforms only NSS solution (Fig. 5a,d) shows a similar trend compare to other nuclear explosions, such as the NTS events and the two DPRK tests (Ford *et al.*, 2010), with the best-fitting full moment tensor solution plotting near the theoretical opening crack mechanism and there being a trend in the best fitting region extending to the negative CLVD. The shaded contour regions correspond to different scaled variance reduction (sVR) in which the sVR in Figure 5 is scaled to the moment tensor solution in the NSS that has the maximum VR. Moment tensor solutions fitting ≥ 90% sVR covers the upper right half of the Hudson source type plot, whereas solutions fitting ≥ 98% sVR wraps around a small region around the theoretical opening crack and includes the best fitting mechanism from the full moment tensor inversion. In the case of using just the waveform data, source mechanisms without a significant explosive component can fit the observed data just as well as a predominantly explosive mechanism (Fig. 5a,d). However, when regional and teleseismic P-wave (Fig. 6) first motions are included in the computation of the NSS a solution that is predominately explosive is obtained (Fig. 5b,e). The NSS results show significant improvement in discrimination capabilities when we included additional constraints from P-wave first motions, especially for moment tensor solutions fitting better than sVR of 90%. Figure 5c,f suggests including just the regional P-wave polarity measurements from the same four stations used in the waveform inversion can greatly increase discrimination capabilities, which is good since good teleseismic data may not always be available. The additional constraints from P-wave first motions eliminate the common ISO-CLVD tradeoff as well as the mechanisms that do not agree with both the higher frequency polarity data and the long period waveforms.

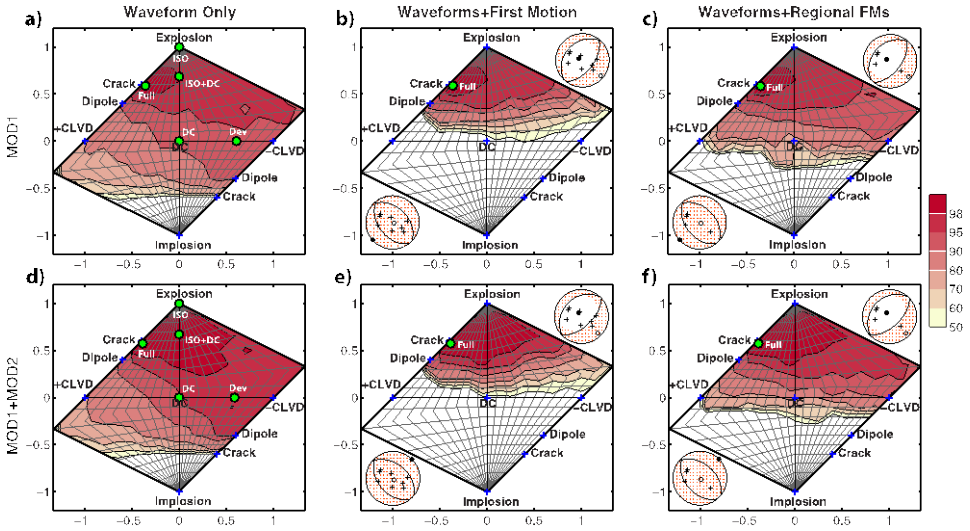

Figure 5. Network Sensitivity Solutions (NSS) for the 1988 Soviet JVE. *Circles are source mechanisms from Figure 4; crosses are the theoretical mechanisms; shaded regions are full moment tensor solutions contoured according to their scaled variance reduction (sVR). Best fitting full and deviatoric mechanisms are also plotted. Black crosses, open circles and circles plotted on top are P-wave up first motions, T- and P-axes.* ***a-c)*** *NSS using MOD1.* ***d-f)*** *NSS using MOD1 and MOD2.*

15 May 1995 Lop Nor Shaft Explosion

In contrast with the 1988 Soviet JVE, the Lop Nor events studied here had only three available regional stations with adequate signal-to-noise in the intermediate- to long-periods employed by our method, and therefore this case presents a very sparse monitoring scenario. We used broadband waveform data filtered between 30 to 50 seconds period from three stations in Eastern Kazakhstan, Eastern Kyrgyzstan and Central Siberia. For the furthest station TLY in Siberia we used a simple layer over halfspace velocity model, NE. This model was obtained using forward and inverse modeling of a local earthquake in Lop Nor, the same earthquake used to obtain MOD1. We used the iasp91 crustal velocity as a starting model, and from our modeling result we observe that because of the distance and long periods the waves are not sensitive to the finer details of the velocity model, and additional layers to the halfspace model do not improve the waveform modeling results significantly. For station AAK in Kyrgyzstan we used MOD1, and for station MAK in Kazakhstan we tested both MOD1 and MOD2. The original instrument response file for MAK from IRIS resulted in anonymously low waveform amplitudes. After comparing the coda envelope functions with nearby stations we concluded the original response file could not be used because the amplitude of the coda envelope function for MAK is significantly shifted from all other nearby stations, indicative of a problematic instrument response. Rautian and Khalturin (1978) observed that coda envelope functions decay stably over time, and amplitudes only vary from event to event. Instead we used a response file from the previous date for the analysis. The first motion picks for the 1995 Lop Nor event are all from regional stations obtained through IRIS, including the three stations used in the moment tensor inversion (Fig. 6).

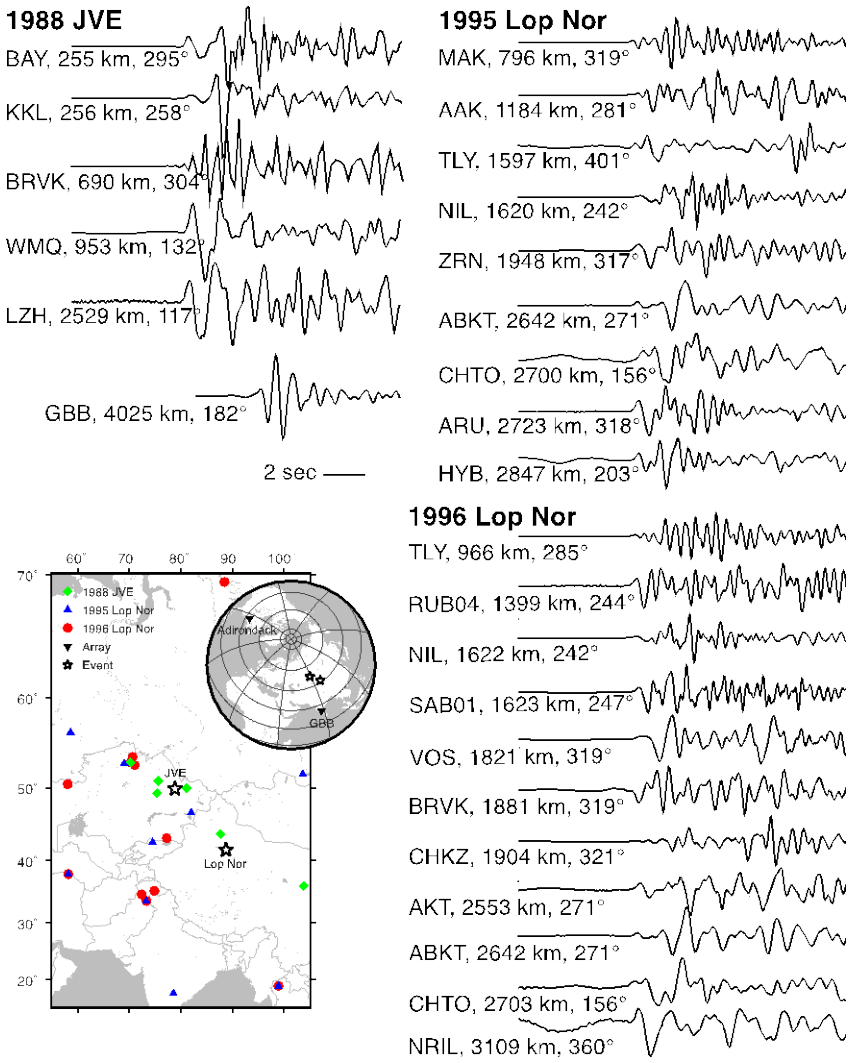

Figure 6. P-wave first motions for the earthquake and two explosions. *The waveforms are bandpass filtered between 0.2 to 3 Hz, except BRVK for the 1988 JVE, which is filtered between 0.2-1.5 Hz to avoid exceeding the Nyquist frequency. P-wave polarities at KSU and the Adirondack array data not shown here (used in the JVE analysis) are from Figure 3 in Priestley et al. (1990) and Figure 12 in Battis and Cipar (1991), respectively. All waveforms are in velocity except for the 1988 JVE event, which is in displacement. Map shows the distribution of stations and array beams for the three events. Gauribidanur array beam (GBB) is filtered between 0.8-5 Hz.*

The best fitting full moment tensor is a predominantly explosive mechanism and has comparable VR to the deviatoric, DC and DC+ISO mechanisms, but a pure ISO source does not fit well. Respective VRs for a full, deviatoric, DC, DC+ISO and ISO mechanisms are 81-86%, 76-78%, 73-74%, 74-78%, and 10%, depending on the velocity model used for MAK. A pure explosive source cannot generate Love waves to fit the large observed Love wave amplitudes on the tangential component, and therefore the pure explosion model has the anonymously low VR of 10% (Fig. 7a). This is of concern since natural tectonic earthquakes represented by a DC actually fit better than the pure

explosion, however in similarity to the JVE, a pure DC solution has the poorest VR compared to other decompositions that include an isotropic component (excluding a pure ISO source). Difficulty fitting the relatively small Rayleigh waves on radial and vertical components at AAK is likely caused by Love wave multipathing based on the particle motions. Surface waves on the radial and vertical components exhibit horizontally polarized Love wave particle motion. The best fitting full moment tensor solution is located near the opening crack mechanism on a Hudson source type plot. This result is consistent with the JVE event and previously studied nuclear explosions (Ford *et al.*, 2010). The waveform only NSS results show a wide range of possible sources fitting ≥ 90% of the best fitting moment tensor solution (Fig. 7b,d), which is largely the result of the large Love wave amplitudes and the sparse station coverage. However, if we use both waveform data and P wave polarities observed at regional distances we see the combined analysis significantly reduces the distribution of solutions with high sVR (≥ 90%) and uniquely discriminates the event as consistent with other nuclear explosions and inconsistent with earthquakes and collapses (Fig. 7c,e). Figure 7c,e shows that the double-couple and deviatoric mechanisms that can fit the surface wave data well fail to fit the first motions at the sites. Velocity model variations also show some variation in the NSS as expected; however, the distribution of sources fitting ≥ 98% of the best fitting solution is similar for both velocity models illustrating that the approach is capable of source type discrimination even in cases where the earth structure is not as well constrained.

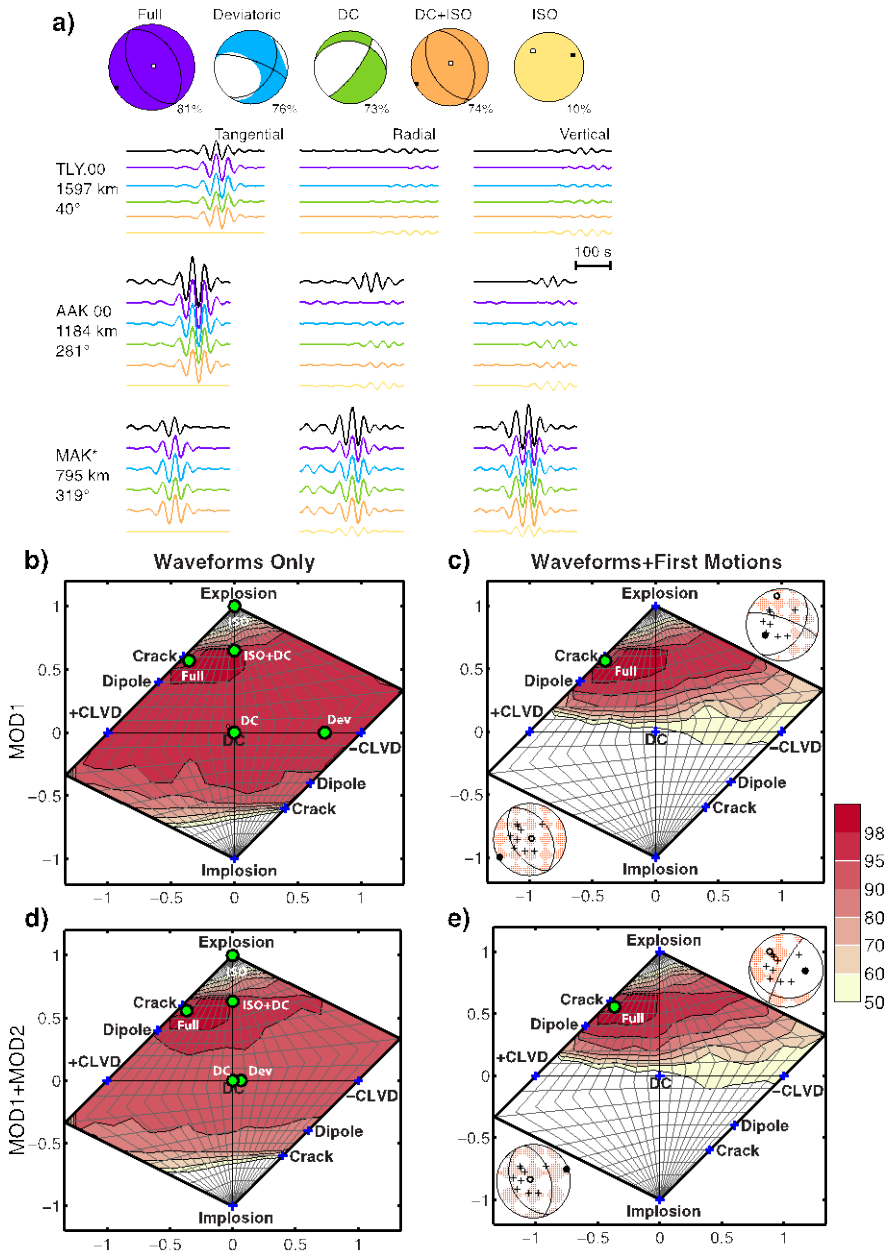

Figure 7. **a)** 1995 Lop Nor Source Model and Waveform Comparisons. *The top trace is the observed waveform data and synthetic waveforms according to their corresponding source mechanisms. Associated variance reduction (VR) for each source type is plotted next to their focal mechanisms. Data show big Love waves on the tangential components. We show results using Green's functions calculated from MOD1 for MAK.*
Figure 7. **b-e)** Network Sensitivity Solutions (NSS) for the 1995 Lop Nor Explosion. *Circles are best fitting full, deviatoric, pure DC, ISO+DC and pure ISO source mechanisms; crosses are the theoretical mechanisms; shaded regions are full moment tensor solutions contoured according to their scaled variance reduction (sVR). Crosses, open circles and filled circles plotted on top are P-wave up first motions, T- and P-axes.*
Figure 7. **b-c)** NSS using MOD1; Figure 7. **d-e)** NSS using MOD1 and MOD2.

8 June 1996 Lop Nor Shaft Explosion

For the second Lop Nor event we used regional waveform data from three broadband stations MAK in Kazakhstan, AAK in Kyrgyzstan, and TTB02 in northeastern Pakistan, and displacement data and synthetics are filtered between 30 to 50 seconds, 30 to 80 seconds and 30 to 50 seconds, respectively. For AAK and TTB02 we used MOD1 to calculate the Green's functions, and for MAK we used both MOD1 and MOD2 since its location falls within the surface tomography study of Sun *et al.* (2010). We used P-wave first motions at regional distances and one station at teleseismic distances (Fig. 6). All stations are obtained from IRIS. The qualities of the picks are good and most show impulsive upward P-wave first motions on the vertical components. The 1996 Lop Nor event has a slightly smaller mb of 5.9 reported in the catalog compared to the 1995 Lop Nor event, which has an mb of 6.1. The M_W from the regional moment tensor inversion is around 5.2 depending on the velocity models used (Table 1). Similar to that of the 1995 event we observe significant Love waves on the tangential component. Because of the strong Love waves the goodness of fit between data and synthetic for a pure ISO solution could not fit the data well (<10% VR) and the best fitting mechanism is an implosion instead of an explosion. To further explore how a pure isotropic solution fits the data, we searched for the best fitting isotropic mechanism using the vertical displacement only. A pure implosion mechanism fits station TTB02 and AAK at 44% VR and 51% VR, respectively with a seismic moment of 1.7×10^{22} dyne-cm, but does not fit station MAK, in fact the synthetic is phased-shifted by $\pm\pi$ from the data. Significant contribution from non-isotropic sources resulted in poor fits to the data when we assume a purely isotropic source. It is possible that the tectonic release for this event is large and likely caused Rayleigh wave reversals (Toksöz and Kehrer, 1972; Ekström and Richards, 1994) thus the pure ISO mechanism is more implosive rather than explosive (Fig. 8a). Rayleigh wave reversals due to large tectonic release have been observed in other nuclear explosions as well, such as the 1998 Indian test (Walter and Rodgers, 1999).

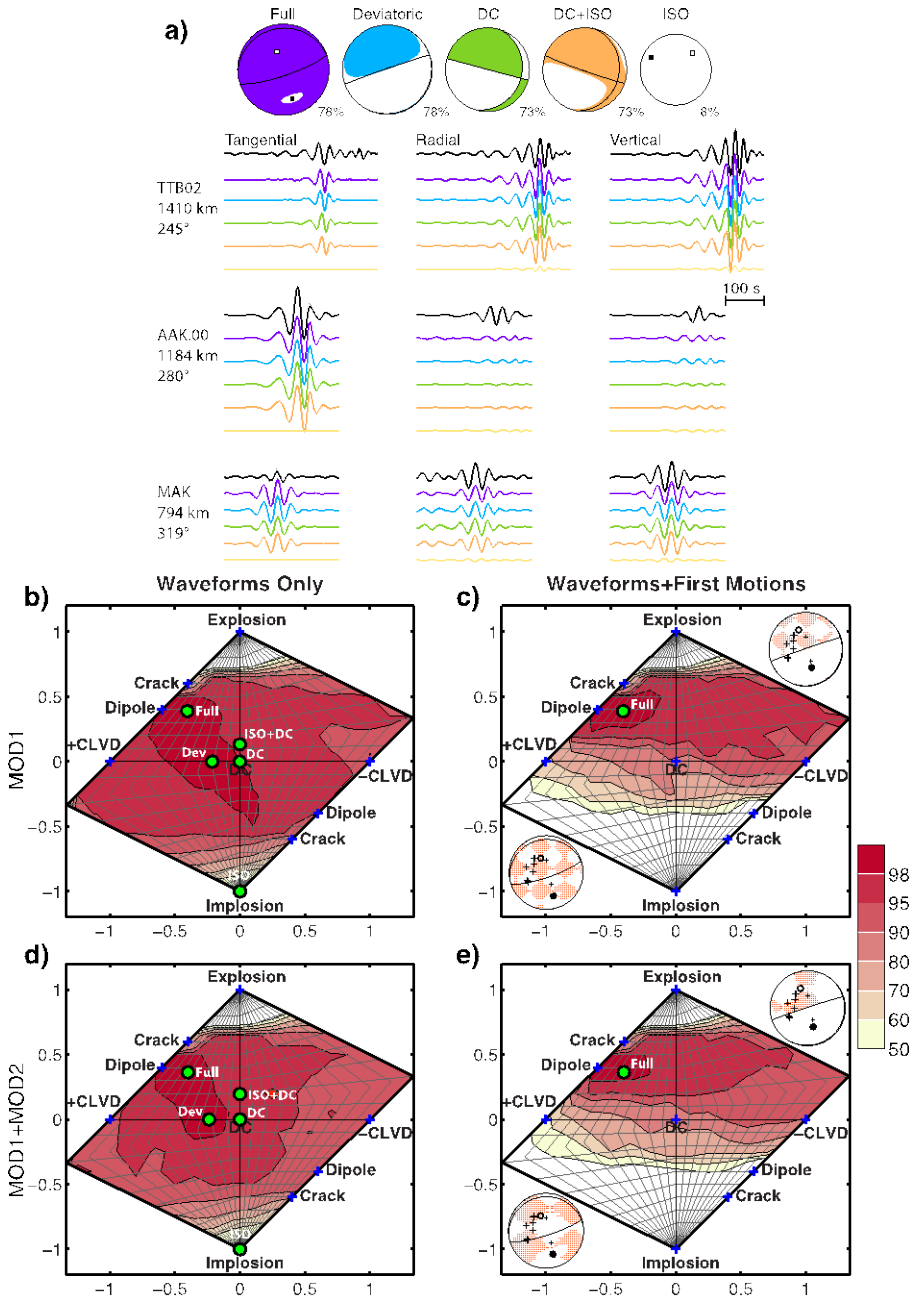

Figure 8. **a)** 1996 Lop Nor Source Model and Waveform Comparisons. *The top trace is the observed waveform data and synthetic waveforms according to their corresponding source mechanisms. Associated variance reduction (VR) for each source type is plotted next to their focal mechanisms. Data shows big Love waves on the tangential component. We show results using Green's functions calculated from MOD1 for MAK.*
Figure 8. **b-e)** Network Sensitivity Solutions (NSS) for the 1996 Lop Nor Explosion. *Circles are best fitting full, deviatoric, pure DC, ISO+DC and pure ISO source mechanisms; crosses are the theoretical mechanisms; shaded regions are full moment tensor solutions contoured according to their scaled variance reduction (sVR). Crosses, open circles and filled circles plotted on top are P-wave up first motions, T- and P-axes.*
Figure 8. **b-c)** NSS using MOD1; Figure 8. **d-e)** NSS using MOD1 and MOD2.

The full and deviatoric solutions for the 1996 Lop Nor event have comparable VR at 78% but are not significantly higher than the best fitting pure DC and ISO+DC mechanisms that have VR at 73% (Fig. 8a). However, a vertical dip-slip mechanism is an uncommon shallow crustal earthquake. The majority of near-vertical or sub-horizontal dip-slip mechanisms in the GCMT catalog are associated with subduction and spreading centers. We expect the waveform only NSS result cannot uniquely discriminate the 1996 event as a predominantly explosive source due to the strong Love waves and sparse station coverage. This is indeed the case and the waveform only NSS shows many different moment tensor solutions have high sVR $\geq$ 90%, and although the NSS contours with sVR $\geq$ 98% includes mostly explosion-like mechanisms it also extends downward and crosses into the horizontal deviatoric axis that is not observed in the 1996 event (Fig. 8b,d). This behavior is likely due to Rayleigh wave reversal. However, after we incorporated regional P-wave first motions the combined NSS results now show similar trends as observed in the 1995 Lop Nor test and the 1988 Soviet JVE, though the difference is contours showing solutions with sVR $\geq$ 90% are more extensive and cross slightly over to the horizontal deviatoric line (Fig. 8c,e). Although the 1996 Lop Nor combined waveform and first motion NSS does not give a unique discrimination, it identifies the source as non-DC. Unlike earthquakes, the distribution of moment tensor solutions is not situated around the pure DC mechanism but shifted along the vertical volumetric axis and towards an opening dipole. The best fitting full moment tensor for the 1996 Lop Nor explosion lies close to the opening dipole, whereas for the Lop Nor earthquake the solution lies close to the DC. Although the 1996 Lop Nor event is not uniquely discriminated as a predominantly explosive source, NSS shows the event is unusual and unlike a typical earthquake that needs further analysis to fully characterize its source process. The earthquake shown in Figure 9 is one of earthquakes used to obtain MOD1, located close to the Lop Nor test site and at 17 km depth. Five stations were available in Eastern Kazakhstan and central Siberia for the inversion (Fig. 9a) and NSS (Fig. 9b-c) but the data are nosier compare to the explosion data.

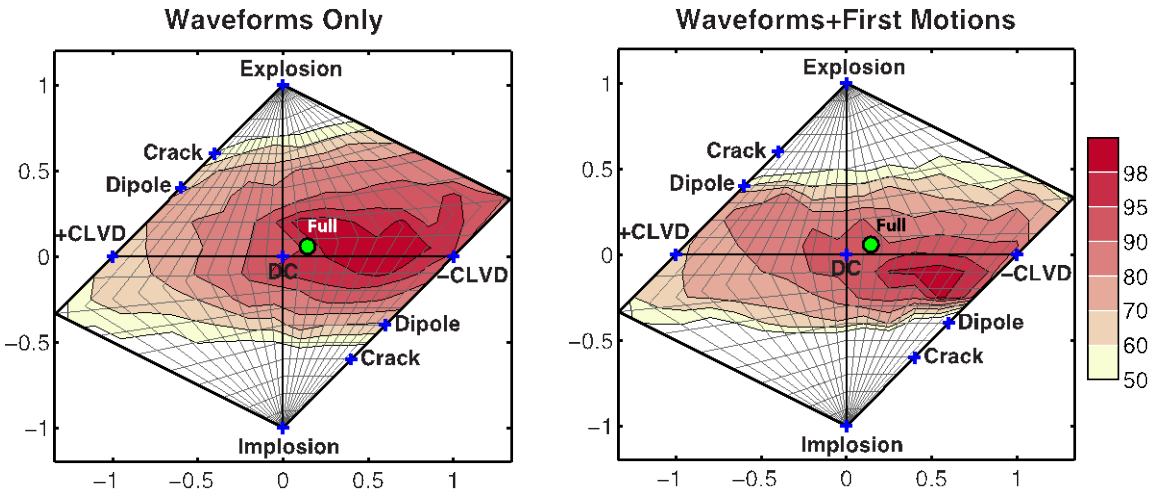

Figure 9. Waveform fits and Network Sensitivity Solutions (NSS) for the 30 January 1999 Earthquake near the Lop Nor Test Site. *The distribution of solutions resembles the Little Skull Mountain aftershock (Ford et al., 2010) but the center of the bullseye is shifted to the right towards the negative CLVD. The station coverage is slightly better than the Lop Nor explosions with additional stations to the west, giving better azimuthal coverage.*

Sensitivity to Station Geometry and Source Depth

Manmade explosions are conducted at shallow depths. For the 1988 Soviet JVE we used a source depth of 1.0 km and for the two Lop Nor shaft explosions we used initial source depths reported in Waldhauser *et al.* (2004), which were estimated using the relationships between mb, yield, and source depth. To test our method's sensitivity to source depth we performed regional waveform moment tensor inversion using a suite of Green's functions calculated at source depths ranging from 0.2 km to 16 km. Unlike tectonic earthquakes, explosions have much shallower source depth, generally < 1 km. Therefore, source depth can be a very useful discriminant for earthquakes and explosions.

Plotting all of the best fitting full moment tensor solutions with additional constraints from P-wave first motions at different depths on a Hudson source-type plot (Fig. 10), we see the sVR gets much worse as source depth increases. The 1988 JVE and 1995 Lop Nor event solutions with high sVR and shallow depths (< 1 km) are centered at the theoretical opening crack mechanisms. In comparison, source depth for the 1996 Lop Nor event is less constrained. Higher uncertainty from the Green's functions (path between the event and station TTB02) and possibly greater tectonic release for this event may have resulted in less sensitivity to source depth. We did not specifically model the path between the event and station TTB02, hence greater errors may be introduced into the calculation of the Green's functions. Although the 1996 Lop Nor event source depth is not as well constrained as the other two events in this paper, most of the high VR solutions are shallow and the mechanisms are close to an opening linear vector dipole. Solutions at greater depths are not explosive but also have lower VR.

In addition to depth sensitivity, we also performed Jackknife tests for the three events to discern the inversions' sensitivity to station geometry. The Jackknife tests reveal we need at least three stations to have confidence in the moment tensor solution. Solutions obtained using less than three stations are not stable, and depending on station geometry can give you incorrect source mechanism. Generally moment tensors computed using stations closer to the source (~300-700 km, as in the case of JVE) resolve more isotropic component and can better constrained the NSS, regardless of the total number of stations used in the inversion.

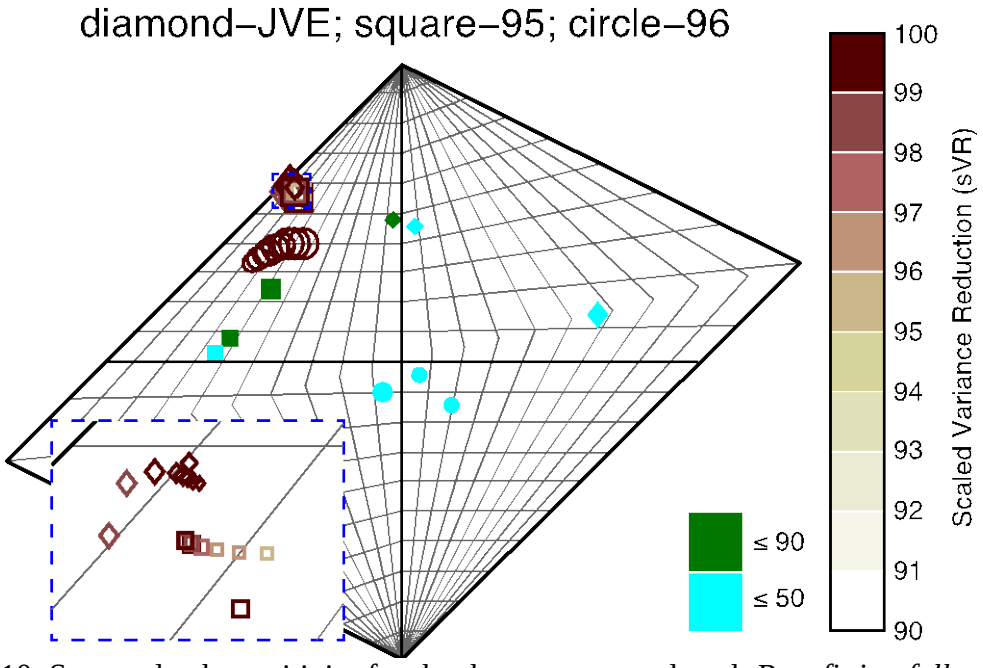

Figure 10. Source depth sensitivity for the three events analyzed. *Best-fitting full moment tensors for the 1988 JVE (diamond), 1995 Lop Nor (square), and 1996 Lop Nor (circle) based on regional waveform inversion and P-wave first motion constraints. Size of the symbol increases with decreasing source depth, filled symbols have sVR ≤ 90%, and open symbols have sVR > 90%.*

Effects of Tectonic Release and Source Medium Damage

The presence of shear waves in seismic recordings of nuclear explosions indicates the explosion process is complex and involves other source processes such as interactions with the free-surface, the effects of shockwave and relaxation of tectonic strain (Patton and Taylor, 2011; Toksöz *et al.*, 1965; Toksöz and Kehrer, 1972; Burger *et al.*, 1986; Day *et al.*, 1987). Recent studies (Ben-Zion and Ampuero, 2009; Patton and Taylor, 2011) have suggested that significant contributions to the radiated seismic wavefield can arise from source medium damage. Material damage associated with explosions affects the Rayleigh wave radiation pattern (Patton and Taylor, 2008), therefore damage may have significant implications to source-type discrimination. Our combined waveform and first motion analysis of the Lop Nor tests shows the regional moment tensor is a promising method for source-discrimination even when tectonic release is large. The best fitting solutions located in the region between a pure explosion and tensile crack on the

source type diagram is comparable to solutions for the DPRK (Ford *et al.*, 2009b; Ford *et al.*, 2010) and NTS explosions (Ford *et al.*, 2009a), and is consistent with the nature of tensile damage above the shot point due to spall and other free surface interactions as proposed by Patton and Taylor (2008). To further assess the capabilities of regional moment tensors for events with tectonic release or source damage, we conducted a series of synthetic tests to examine these effects.

Two types of composite sources were tested: (1) a ISO + DC source and (2) a ISO + CLVD source. The ISO + DC source examines the effects of tectonic release and consists of an explosion and a 45-degree dipping reverse fault mechanism. The ISO + CLVD source examines the effects of source medium damage and consists of an explosion and a CLVD mechanism with a vertically oriented major vector dipole (Patton and Taylor, 2008). To describe the relative seismic moments between the different source types, we used the relationships proposed by Toksöz *et al.* (1965) for tectonic release and Patton and Taylor (2008, 2011) for material damage from a deviatoric source. The index F measures the ratio between isotropic moment (M_{ISO}) and double-couple moment (M_{DC}),

$$F = 1.5\frac{M_{DC}}{M_{ISO}} \tag{6}$$

The index K measures the relative strengths of the moment tensor elements,

$$K = \frac{2M_{XZ}}{M_{XX} + M_{YY}}, \tag{7}$$

and when tectonic release occurs only in the horizontal plane as in our second test case,

$$K = \frac{2\left(M_{ISO} + M_{CLVD}\right)}{2M_{ISO} - M_{CLVD}}, \tag{8}$$

We used the 1988 Soviet JVE station geometry and Green's functions from our moment tensor analysis to compute the synthetic data, and added real noise collected from the stations used in the Soviet JVE analysis or from other nearby IRIS stations when pre-event seismic recordings are not available. For the two composite sources (ISO+DC and ISO+CLVD) we tested different F-factors and K-factors, and for each factor we looked at different SNRs at 5%, 10%, 15% and 20% of the maximum vertical Rayleigh wave amplitude. We performed the synthetic testing using long period waveforms only, and another one combining the waveforms and four P-wave first motion measurements recorded at the same seismic stations. For the remaining part of this section we focused on results from the tests where SNR is 20% of the maximum vertical Rayleigh wave amplitude. This is the most extreme case of SNR and generally the real data we use have SNR levels that are much lower than 20%. The distribution of individual moment tensor solutions ≥ 98% sVR in the Hudson source-type diagram are more compacted for lower

SNR levels, but the contours outlining all possible points are very similar for all SNR levels. This observation applies to both composite source cases we tested.

The ISO+DC composite source case shows the waveform only NSS becomes more constrained with increasing contribution from tectonic release (Fig. 11). Best-fitting full moment tensor solutions center around the opening crack mechanism, which is consistent with solutions obtained from real explosions. Although this seems counterintuitive, the NSS gives a predominantly explosive source because the contribution from a reverse fault mechanism helps eliminate the well-known ISO-CLVD tradeoff between explosion and -CLVD. The reverse fault radiation pattern is more similar to a +CLVD mechanism. Hence, the two competing mechanisms eliminate the ISO-CLVD tradeoff. Best-fitting full moment tensor solutions of different degree of tectonic release are all near the opening crack mechanism, which is consistent with solutions obtained from real explosions. The waveforms only NSS and combined waveform and first motion NSS show very similar distribution for sVR $\geq$ 98%. We see no significant improvement by adding first motions because the waveforms only NSS already uniquely identifies the source as predominantly explosive. However, first motions do help constrain the NSS for solutions with sVR $\geq$ 90%, due to the fact that the P-wave radiated from the explosion is primary and precedes motions due to secondary block faulting (delay time between explosion and secondary faulting is 1 second), or tensile damage above the shot point. By using both long period waveforms and P-wave polarities we can capture the volumetric signature of the event when tectonic release has significant contribution to the explosion source processes. In the event that we cannot uniquely discriminate the event as explosive, the deviation from deviatoric mechanisms flags the event as uncommon and warrants further analysis to understand its source processes.

To look at the effects of medium source damage, we adopted the model proposed by Patton and Taylor (2008) where the cause of damage is represented by a vertically oriented CLVD source. The deformation observed at the source with this model is extensional along the vertical axis and horizontal compressions around the explosion (+CLVD). As defined by Patton and Taylor (2008), a K-factor of 1 means contribution from CLVD vanishes to zero, K > 1 means extension along the vertical axis, and K < 1 means compression along the vertical axis. Our synthetic tests with just waveform data show K > 1 (implying greater material damage) reduces the commonly observed ISO-CLVD tradeoff (Fig. 12). This is the result of competing mechanisms between the -CLVD and +CLVD, increasing contribution from a +CLVD source mechanism affects the Rayleigh wave radiation pattern thus enhancing the explosive characteristics of the source. In contrast, K < 1 where compressional deformation is along the vertical axis the ISO-CLVD tradeoff persists. In some cases when K is high ($\geq$ 2.5) the NSS identifies the event as explosive even without additional constrains from P-wave first motions. In other cases where the event is not uniquely identified as explosive, additional P-wave first motions improve the solution by shifting the 98% sVR contours above the deviatoric CLVD mechanism and reducing the region of possible source mechanisms.

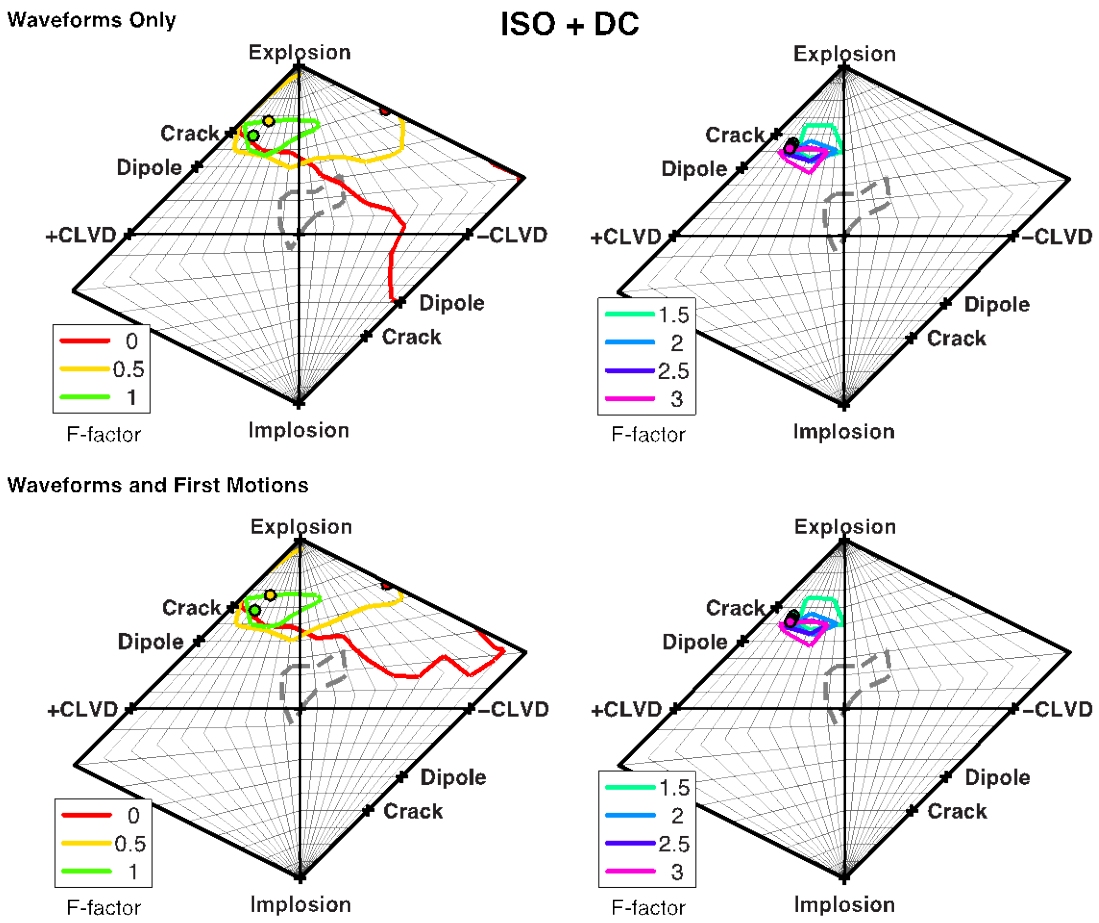

Figure 11. Network Sensitivity Solutions (NSS) for an ISO+DC composite source. *Plotted are the 98% scaled variance reduction (sVR) contours with increasing F-factor (therefore increasing contribution from the DC component), and dashed contours are from a pure reverse fault (DC) mechanism. The circles are the best fitting full moment tensor solution from waveform inversion. Here we compare how the NSS changes when additional P-wave first motions are included.*

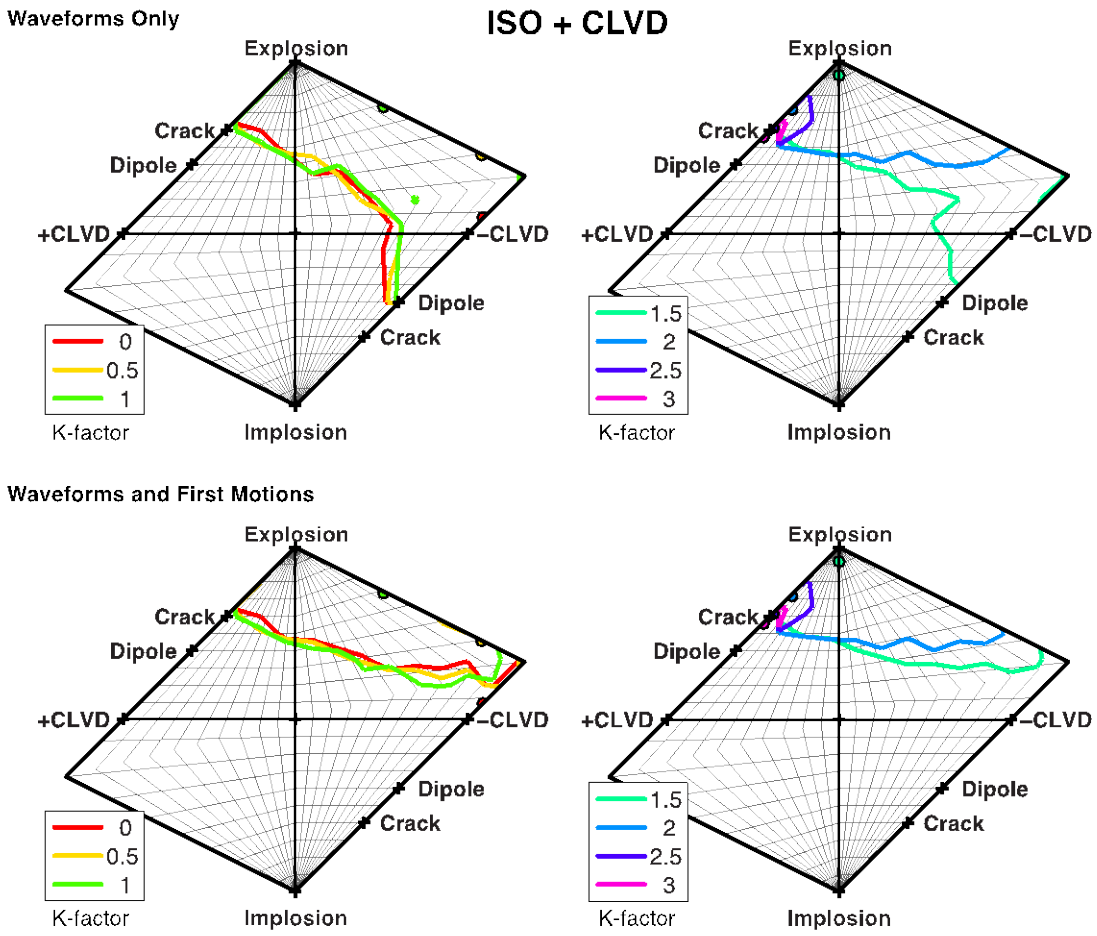

Figure 12. Network Sensitivity Solutions (NSS) for an ISO+CLVD composite source. *Plotted are the 98% scaled variance reduction (sVR) contours with increasing K-factor (therefore increasing contribution from the CLVD component). The circles are the best fitting full moment tensor solution from waveform inversion. Here we compare how the NSS changes when additional P-wave first motions are included.*

Conclusions

We have performed seismic moment tensor inversions for the 1988 Soviet JVE test and two Lop Nor nuclear tests. These cases represent sparse monitoring conditions and/or uncertainty in velocity structure. In each case we have shown that the use of long-period waveform data comprised mostly of regional surface waves result in solutions with large isotropic components that are consistent with solutions for other studied nuclear tests (Ford *et al.*, 2009a; Ford *et al.*, 2009b; Ford *et al.*, 2010). Using only regional waveforms, the distribution of solutions on the source type diagram of Hudson *et al.* (1989) do not cleanly discriminate the event either because of the known explosion negative CLVD tradeoff (case of the JVE event) or due to large observed Love waves (cases of the two Lop Nor tests). In each case, however, the inclusion of regional P-wave polarities, and ideally observations from teleseismic arrays when available, reduces the

area of solutions that provide a good level of fit to the data, providing good separation from double-couple solutions and solutions on the deviatoric line.

The 8 June 1996 Lop Nor test indicates that Rayleigh waves may be reversed at some of the regional stations due to a large tectonic release. The large tectonic release is possibly due to shock driven block faulting or tensile damage (Patton and Taylor, 2008). To further investigate this we carried out a series of synthetic tests using the JVE station geometry to evaluate the regional moment tensor method capabilities for different levels of tectonic release measured by both the Toksoz F index and the Patton K index. These tests show that the combination of long-period regional waveform data and regional distance P-wave first motions are able to resolve the anomalous volumetric nature of compound explosion tensile damage and block faulting events.

This work has been published in the Bulletin of the Seismological Society of America (Chiang et al., 2014).

3.3. Analysis of the Effects of Vanishing Traction on Seismic Moment Tensor Recovery for Shallow Explosions

Introduction

For the nuclear explosion source-type identification problem the uncertainty in a solution is as important as the best fitting parameters. A potential issue for shallow seismic sources that are effectively at the free-surface between the ground and air is that the vanishing traction at the free-surface can cause the associated vertical dip-slip (DS) Green's functions to have vanishing amplitudes (Julian et al., 1998), which in turn can result in the indeterminacy of the M_{xz} and M_{yz} components of the moment tensor and therefore bias in the moment tensor solution. The effects of the free-surface on the stability of the moment tensor becomes important as we continue to investigate and improve the capabilities of regional full waveform moment tensor inversion for source-type identification and discrimination. It is important to understand its effects for discriminating shallow explosive sources for nuclear monitoring, but could also be important in natural systems that have shallow seismicity such as volcanic environments and geothermal systems, and other manmade shallow seismicity related to anthropogenic activities such as hydraulic fracturing and mining.

To tackle the potential issues that could arise in the moment tensor analysis of shallow sources, we performed a series of synthetic tests to understand the effects of free-surface vanishing traction on the total seismic moment, isotropic seismic moment and the source mechanism. We evaluate the sensitivity of the moment tensor solutions as a function of source depth and velocity model. Based on what we learn from the synthetic studies, we applied the moment tensor method to the HUMMING ALBATROSS quarry blast events, which is an excellent dataset in terms of understanding the effects of free-surface vanishing traction in real seismic recordings. These small chemical explosions are approximately 10 m deep and are recorded at up to several km distances. Therefore the data represent a rather severe source-station geometry in terms of vanishing traction issues. It is possible to obtain a robust full moment tensor solution that is comprised dominantly by an isotropic or explosive component, however the data provide the opportunity to evaluate capabilities of moment tensor inversion as a function of both source depth and frequency. The details of the data processing and methodology are similar to that of the JVE and Lop Nor events, as described in section 3.2.

Free-Surface Vanishing Traction

The first step before performing the synthetic analysis is to look at how the fundamental Green's functions behave as source depth decreases. Using the western United States velocity model (Song et al., 1996) we generate the ten fundamental Green's functions at 100-km distance with source depths ranging from 0.2 to 1.2 km. The Green's functions were bandpass-filtered between 10 to 50 seconds period. As shown in Figure 13 there is a strong source depth sensitivity on the vertical dip-slip (DS) fundamental

Green's functions associated with the Mxz and Myz elements for all three components (ZDS, RDS and TDS) in which there is a systematic reduction in displacement amplitude with decreasing source depth. This effect was noted in a study on fundamental Love and Rayleigh waves for nuclear explosions and associated tectonic release (Given and Mellan, 1986). In contrast, the vertical strike-slip Green's functions for all three components (ZSS, RSS and TSS) and the explosion Green's functions for the vertical and radial components (ZEP, REP) show little to no variation in amplitude and waveform with respect to depth. The 45-degree dip-slip Green's functions (ZDD and RDD) show very small variations in waveforms due to the constructive and destructive interference of waves interacting with the free-surface. While the wave interference appears minor in the 10 to 50 second period passband (Figure 13) it is more pronounced in the unfiltered displacement Green's functions.

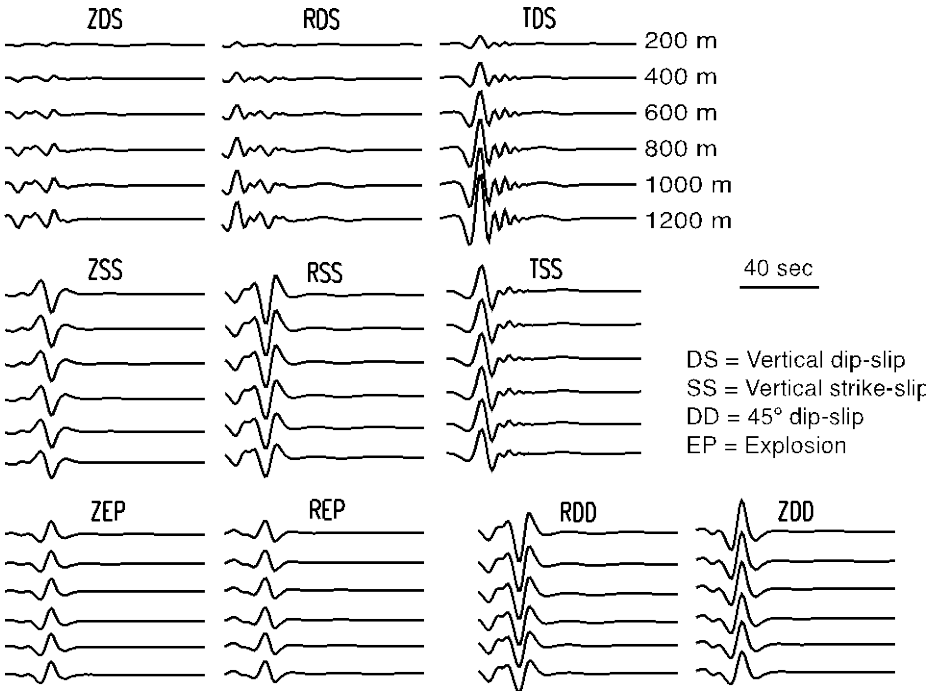

Figure 13. Green's functions (GF) computed using the Song et al., (1996) 1D western U.S. velocity model. *GF are in displacement and filtered between 10-50 second period. The traces for each component, from top to bottom, are at 200, 400, 600, 800, 1000, and 1200 m source depths.*

The low amplitude DS component Green's functions could lead to bias in seismic moment tensor results, particularly when noise in the data is also considered. It is interesting to note however that while there are strong effects on amplitude the waveforms remain similar and there is little effect on the phase of the waveforms on these components. This suggests that it may be possible to develop a correctional term to scale the Green's functions for shallow sources prior to the moment tensor inversion.

In the synthetic study we generated a suite of velocity models by introducing a shallow velocity gradient to the 1D western US reference model (Song et al., 1996). This is accomplished by splitting the top 2.5-km thick layer in the reference model into two

separate layers. We systematically adjust the thickness and velocity of the two new layers (Figure 14), but constrain the variations of the two parameters by maintaining the same vertical travel time as the reference model. The purpose of the study is to generate different but comparable velocity models. For each 1D model, we generated Green's functions at regional distances between 100 and 400 km with source depths ranging from 0.2 to 3.5 km. Using the same set of Green's functions we generated two types of synthetic data with different source mechanisms: 1) a pure explosion case [EXP] and 2) a composite source case (double-couple [DC] and EXP) with an F-factor of 1 (Burger et al., 1986). The synthetic data are computed following the expressions from Minson and Dreger (2008). We added random Gaussian white noise with 20% of the maximum amplitude of the synthetic data, then we use a 10 to 50 second causal bandpass Butterworth filter to filter the synthetic data and the Green's functions. We implemented a semi-ideal four-station coverage for the inversion, consisting of source-to-receiver distances at 100, 200, 300 and 400 km, and distributed in semi-regular azimuths. The linear inversion problem yields six independent components of **M**ij.

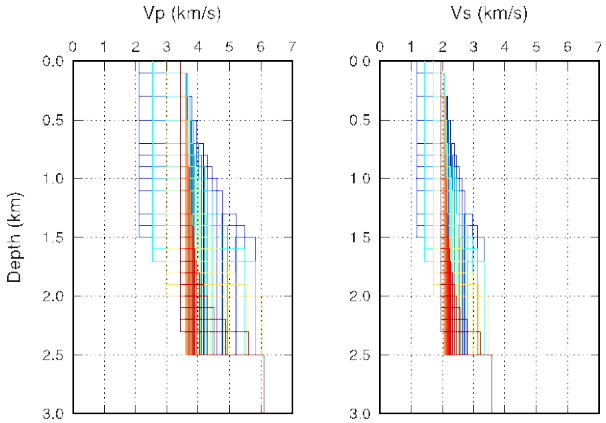

Figure 14. Velocity models derived from the Song et al. (1996) 1D model by keeping the top 2.5-km vertical travel time constant. *The model parameters are the same below 2.5-km depth.*

Of the 59 velocity models tested, those with a shallow velocity gradient in the upper 1.5-km have little to no bias in their isotropic and total moment estimates, and all estimates fall within the 20% noise level for both the explosion source and the composite source. Similarly, moment estimates from models with a shallow velocity gradient in the upper 1.5- to 2.0-km, and at depths greater than 0.4 km, are all within 20% of the input values. Although the total moment estimates for the composite case exhibit greater deviations from the input value at source depths shallower than 0.4 km, the bias in the isotropic moment is less significant (Figure 15). In most cases the full moment tensor inversion successfully recovers the correct mechanism for both the pure explosion case and the composite case over the targeted depth range (< 1 km) for nuclear explosions. Free-surface vanishing traction has little effect on recovering the correct mechanism for models with a shallow velocity gradient. The inversion can still recover the correct mechanism for models without a strong shallow velocity gradient at depths greater than 0.5 km; the bias in source mechanism is significant only at depths shallower than 0.4 km. The key observation from the synthetic tests is the amount of bias in the recovered

moment and source mechanism of very shallow sources depends on the velocity model. Models with a shallow gradient produce more complex Green's functions, and it is possible that the complexities in the waveforms provide more constraints in the moment tensor inversion and so they are more likely to recover the correct solution.

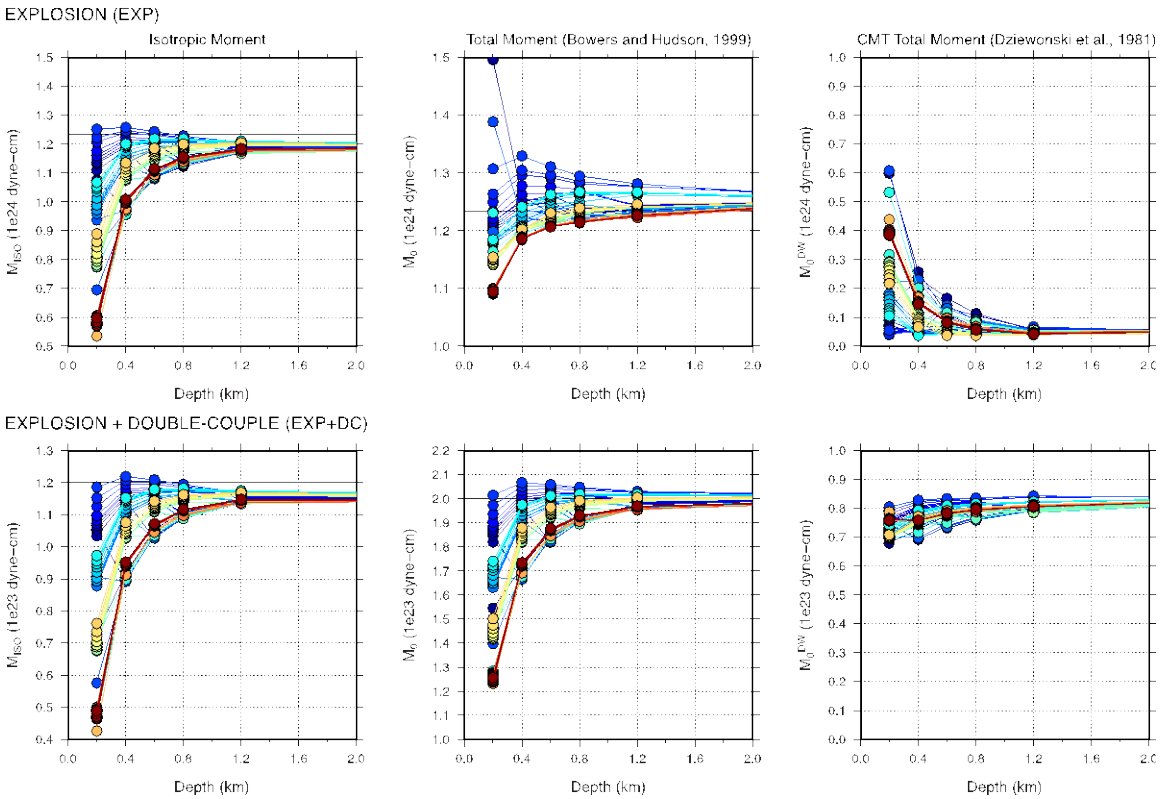

Figure 15. Isotropic moment and total seismic moment for the pure explosion source and composite source, plotted as a function of source depth. *The color corresponds to the different velocity models in Figure 14. Solid black lines are the input/correct seismic moments.*

HUMMING ALBATROSS

The HUMMING ALBATROSS data consist of both broadband and short-period seismic recordings (Figure 16). We applied the moment tensor based discrimination method to two ~M2-2.5 industrial chemical explosions. Following the results of Ford et al. (2012) and Chiang et al. (2014) we incorporated full waveform data from five broadband stations and P-wave first motions from sixteen broadband and short-period stations into our moment tensor analysis. The broadband waveform data are filtered between 0.5 to 2 seconds depending on the signal-to-noise-ratios, and we examined the results in two frequency bands to understand the frequency dependence of free-surface vanishing traction. To further assess the uncertainties in the moment tensor inversion result, we looked at how the solution behaves in the Hudson et al. (1989) source-type space. Following the Network Sensitivity Solution (NSS) method proposed by Ford et al. (2010), we randomly generated 80 million moment tensor solutions that are uniformly distributed on the Hudson source-type plot, and for each random solution we compared

the waveform fits and P-wave first motion picks between the data and synthetics. Here we compare two types of NSS result: 1) waveform data only and 2) combined full waveform and local P-wave polarity data.

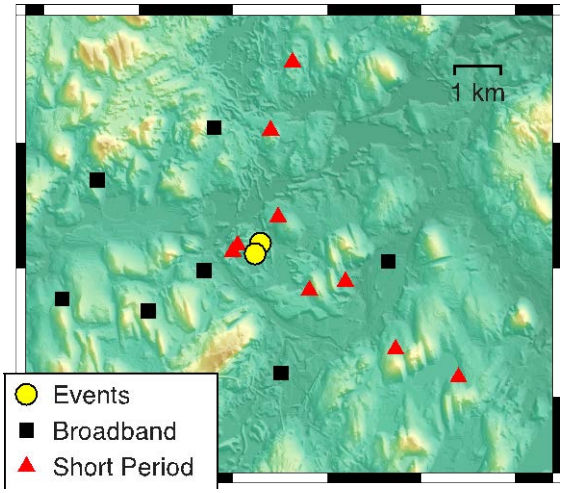

Figure 16. Event (shot) and station locations of HUMMING ALBATROSS. *Background colors represent topography where green is lower elevation.*

Given the frequency band and source-receiver distance, the moment tensor inversion is not sensitive to source depths shallower than ~150 m, but the solutions at these shallow depths remain stable and are dominated by a large isotropic component (Figure 17). This is true for both shots. If we have no prior knowledge on source depth, the sensitivity analysis shows we can constrain the depth to be shallower than ~150 to ~200 m, this depth range is indicative of possible manmade seismicity since natural earthquakes rarely occur at these depths. Because we know the depth of the borehole where the explosions are detonated, we can exclude sources deeper than 15 m. For the subsequent NSS analysis we fixed the source depth at 11 m, where the maximum VR occurs, even though the VR of moment tensor solutions between 5 and 15 m are essentially the same.

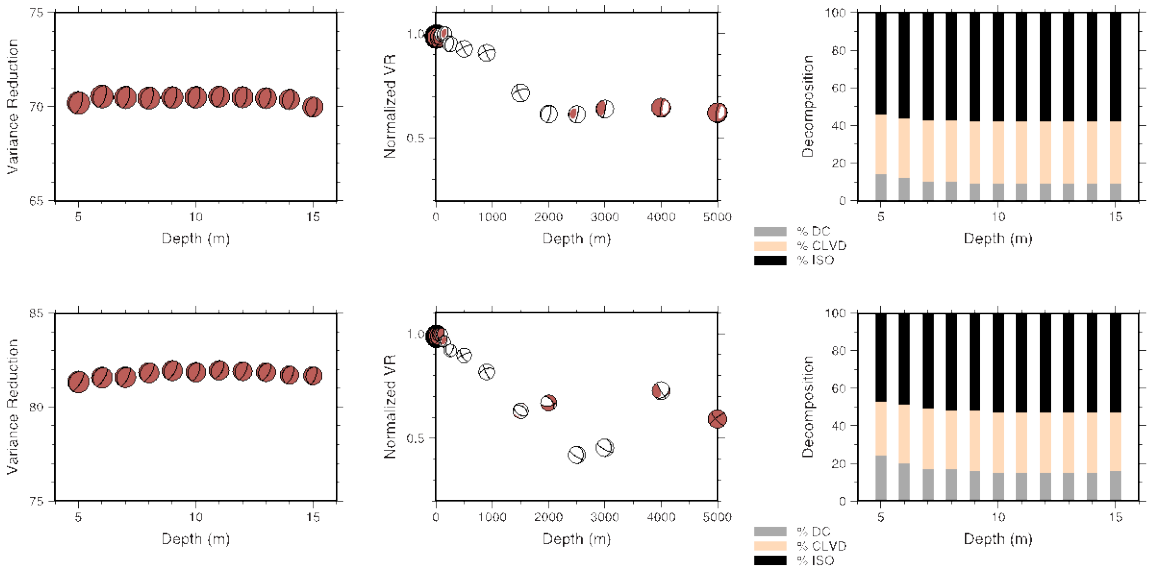

Figure 17. Full moment tensor solutions and decompositions as a function source depth. *The top row shows results from shot one and the bottom row shows results from shot two. Note the x-axes (depth) scales are different.*

The results for both shots are very similar. Shot one has a slightly larger magnitude Mw ranges between 2.5 and 2.9 depending on the frequency band used in the inversion. For Shot two Mw is between 1.9 and 2. The total seismic moment increases when we use longer period waveforms. The waveform NSS exhibits a tradeoff between volumetric sources and double-couple sources (Figure 18). The 98% VR contours wrap around the theoretical DC and extend towards the theoretical opening crack mechanism, but is not as pronounced for shot one at higher frequencies 0.8-2.0 Hz (Figure 18a). This tradeoff is likely caused by the combination of large Love waves on the tangential component and free-surface vanishing traction. The large Love wave causes the solution to deviate from a pure explosive mechanism. Vertical dip-slip and explosive mechanisms fitting equally well to the data (Figure 19) indicates free-surface effects also contribute to the observed tradeoff. The tradeoff becomes more pronounced at longer periods because free-surface effects are more severe at longer wavelengths. The seismic moment also increases when we look at longer period waves.

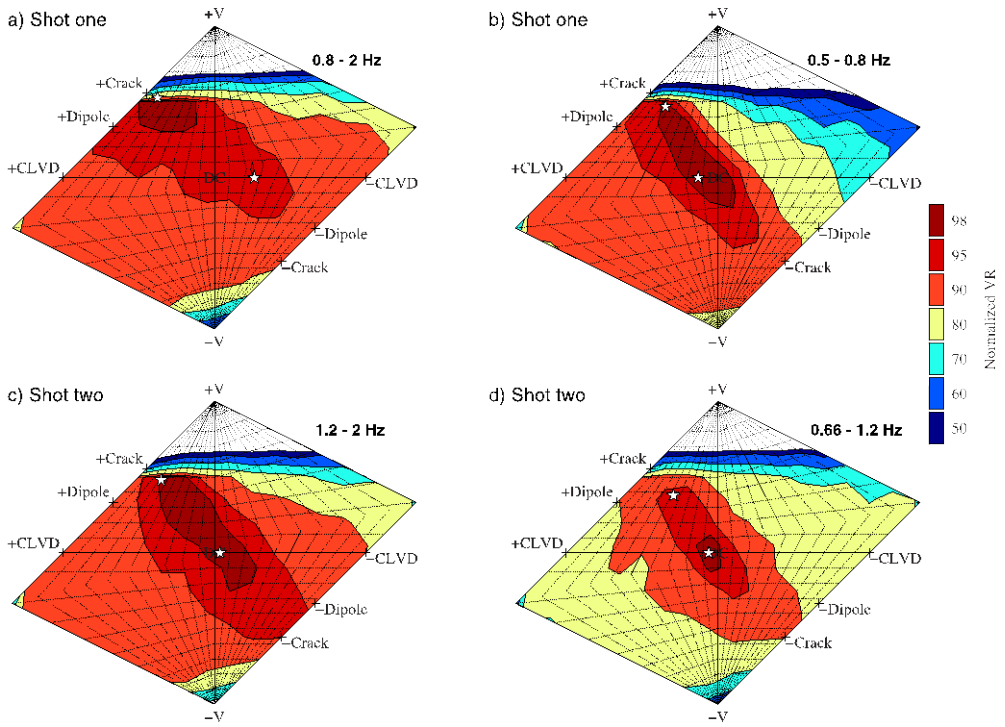

Figure 18. Network sensitivity solutions (NSS) for both shots, at different frequency bands and using only waveform data from five broadband stations. *White stars are the best-fitting full and deviatoric moment tensor solutions from time-domain full waveform inversion.*

Using only the waveforms we cannot constrain the two shots to be explosive as the uncertainties in the NSS encompass non-isotropic mechanisms. To eliminate the tradeoff we applied additional constraints from P-wave first motion polarities (in which all show upward motion), and the resulting NSS's show the best solutions that fit both full waveform and P-wave first motion polarities are constrained to mechanisms with a dominant isotropic or volume increase component, including the full moment tensor solution from waveform inversion (Figures 19 & 20). By incorporating additional P-wave polarity picks from the local network of stations, we now have greater confidence in discriminating the two shots as explosive events. The combined NSS results are equally well constrained for both frequency bands. Once again like the JVE and Lop Nor events, additional P-wave polarity information provides a very important constraint. The P-wave data eliminates mechanisms such as the vertical dip-slip, and discriminates the event as predominantly explosive. The combined results show that the moment tensor method is capable of discriminating very shallow events, where free-surface effects are significant and cannot be ignored.

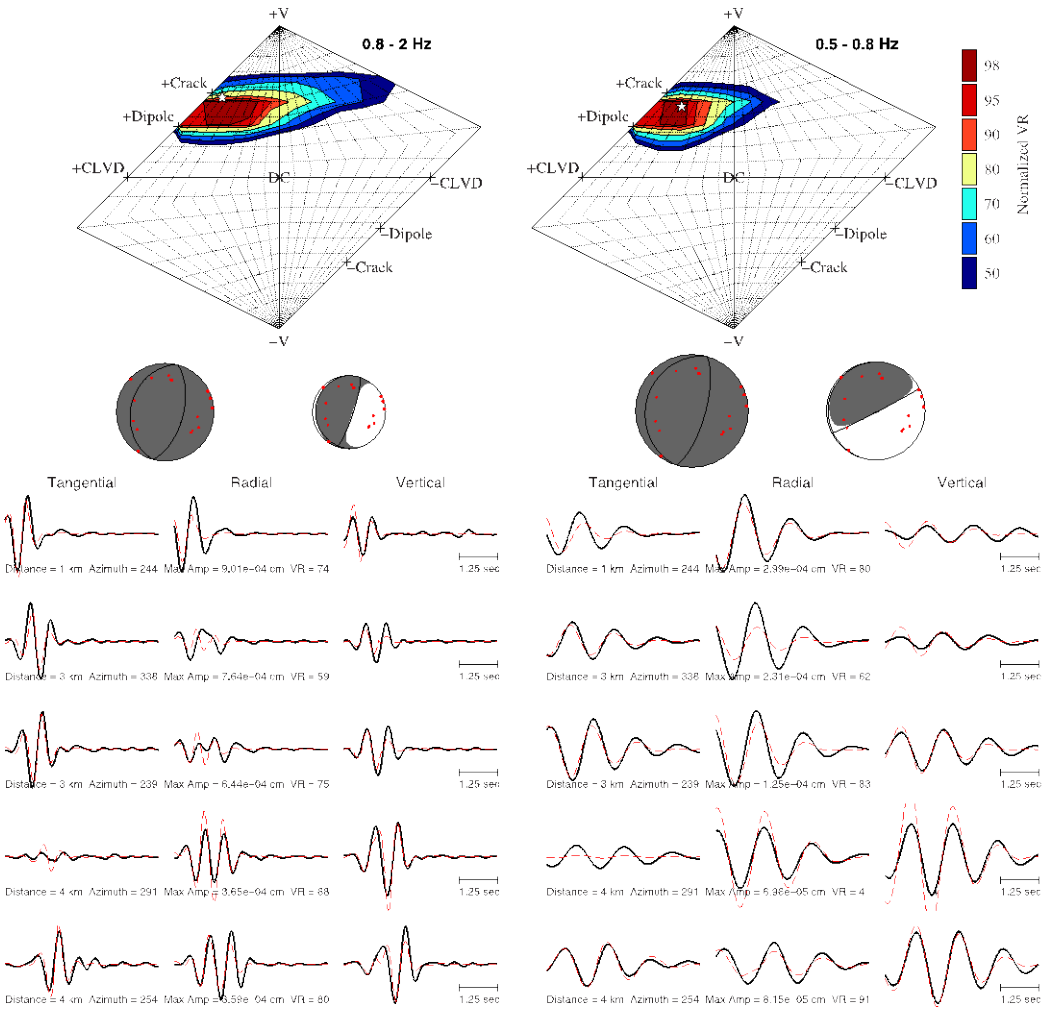

Figure 19. Combined waveform and P-wave first motion polarity NSS for shot one, and the full and deviatoric moment tensor solutions time-domain waveform inversion. *Red dots are upward P-wave first motions from sixteen broadband and short-period stations. The solid black lines are data in velocity and the full moment tensor synthetics are the dashed red lines.*

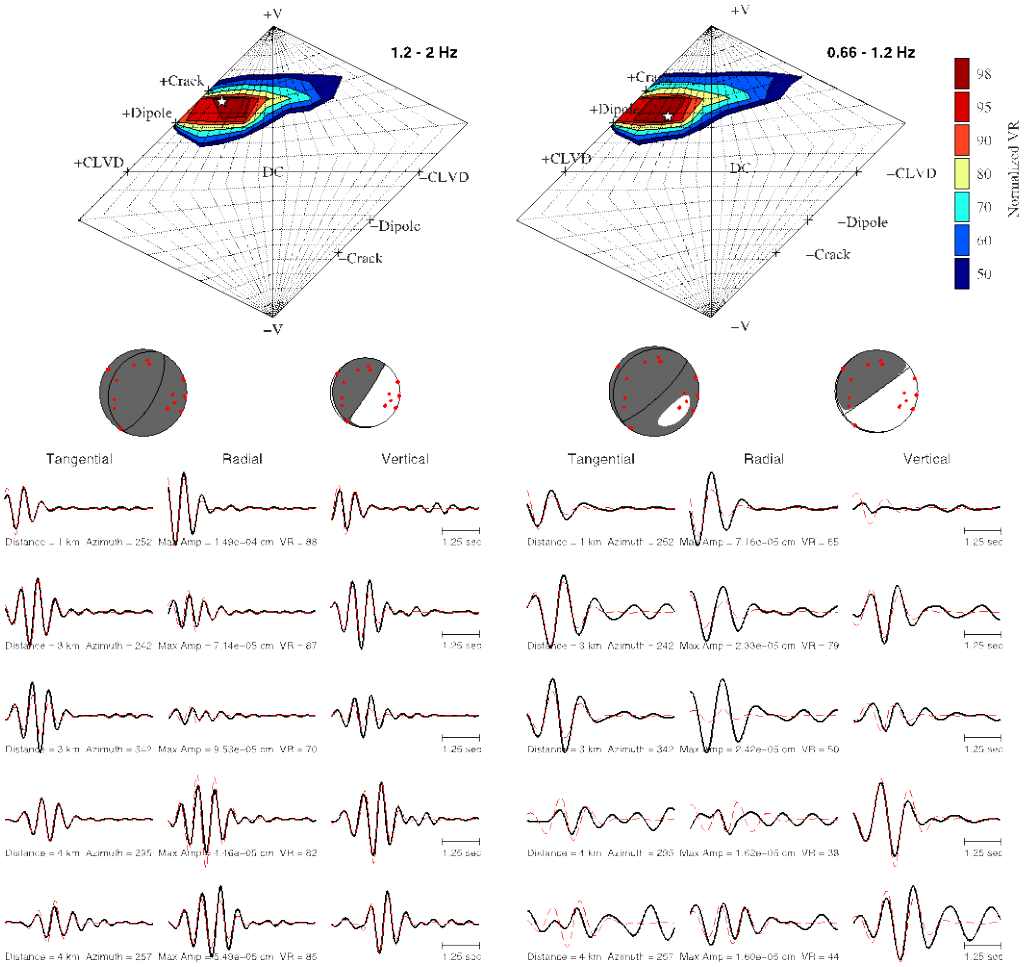

Figure 20. Combined waveform and P-wave first motion polarity NSS for shot two, and the full and deviatoric moment tensor solutions time-domain waveform inversion. *Red dots are upward P-wave first motions from sixteen broadband and short-period stations. The solid black lines are data in velocity and the full moment tensor synthetics are the dashed red lines.*

3.4. A Continuous Scanning Algorithm for Micro-Earthquakes and Shallow Explosions

We have applied a continuous scanning algorithm to determine seismic moment tensors of micro-earthquakes with no a priori information. This method may be applied to streaming data in real time to detect, locate and estimate seismic moment tensors of seismic events. It may also be applied to archived data to investigate large numbers of events in an automated manner. In the following we describe the application of the algorithm to seismicity associated with the collapse of a brine cavern on the side of a salt dome in Louisiana. These events are unusual and display large volume increase components indicating involvement of fluids in the seismic source process. The results also demonstrate that the approach could be used to detect, locate, determine seismic moment tensors, and discriminate explosions from typical earthquakes.

Introduction

Napoleonville Salt Dome (*NSD*) is located at -91.13° E, 30.01° N near Bayou Corne, Assumption Parish, southeast Louisiana (Figure 21). It is a part of the Gulf Coast salt basin which exhibits many salt structures formed by upward flow of sedimentary salt (primarily, evaporites) on account of low density of salt and overburden pressures caused by younger sedimentary deposits (Beckman and Williamson, 1990). It penetrates the Mississippi River Valley Alluvial Aquifer (*MRAA*) zone, which is primarily composed of upper Pleistocene-Holocene sediments, to an approximate depth of 200 m (Beckman and Williamson, 1990). Salt domes are commonly used for solution mining of salt; and caverns thus formed are also used for storage of hydrocarbons and industrial wastes owing to strong impermeability of salt (Thoms and Gehle, 2000). 54 caverns distributed over an area of 1.6 km (*N-S*) to 4.8 km (*E-W*) have been operating in *NSD* at various times since 1950, both for brine mining and storage. Beginning in June 2012, residents of Bayou Corne reported frequent tremors and unusual gas bubbling in local surface water bodies (Report 1, 2013). The parish requested the assistance of the United States Geological Survey (*USGS*) to monitor the continuous seismic activity. A temporary network of seismic stations was set up which revealed a sequence of numerous seismic events (Ellsworth *et al.*, 2012; Horton *et al.*, 2013). On 03 August 2012, a large sinkhole was discovered close to the western edge of the salt dome (Figure 21b) leading to a declaration of emergency and evacuation of nearby residents (Report 2, 2013). The sinkhole, filled with a slurry of water, crude oil and debris, swallowed cypress trees, and its geometry has been actively changing ever since, with recent estimates of surface area being greater than 20,000 m^2, and maximum depth varying between ~ 30 and 100 m over time (Report 1, 2013). Subsidence, intermittent seismicity and bubbling of natural gas have been observed in the affected region. Preliminary investigations suggest that possible collapse of the lower sidewall of a plugged and abandoned brine cavern, *Oxy Geismar* 3, might be a potential cause of the sinkhole (Report 1, 2013; Report 2, 2013). It has been hypothesized that the collapse fractured to the surface, creating a disturbed

rock zone which provides a pathway for formation fluids, natural gas and crude oil from deeper strata that are now accumulating in the sinkhole and the surrounding subsurface (Report 1, 2013).

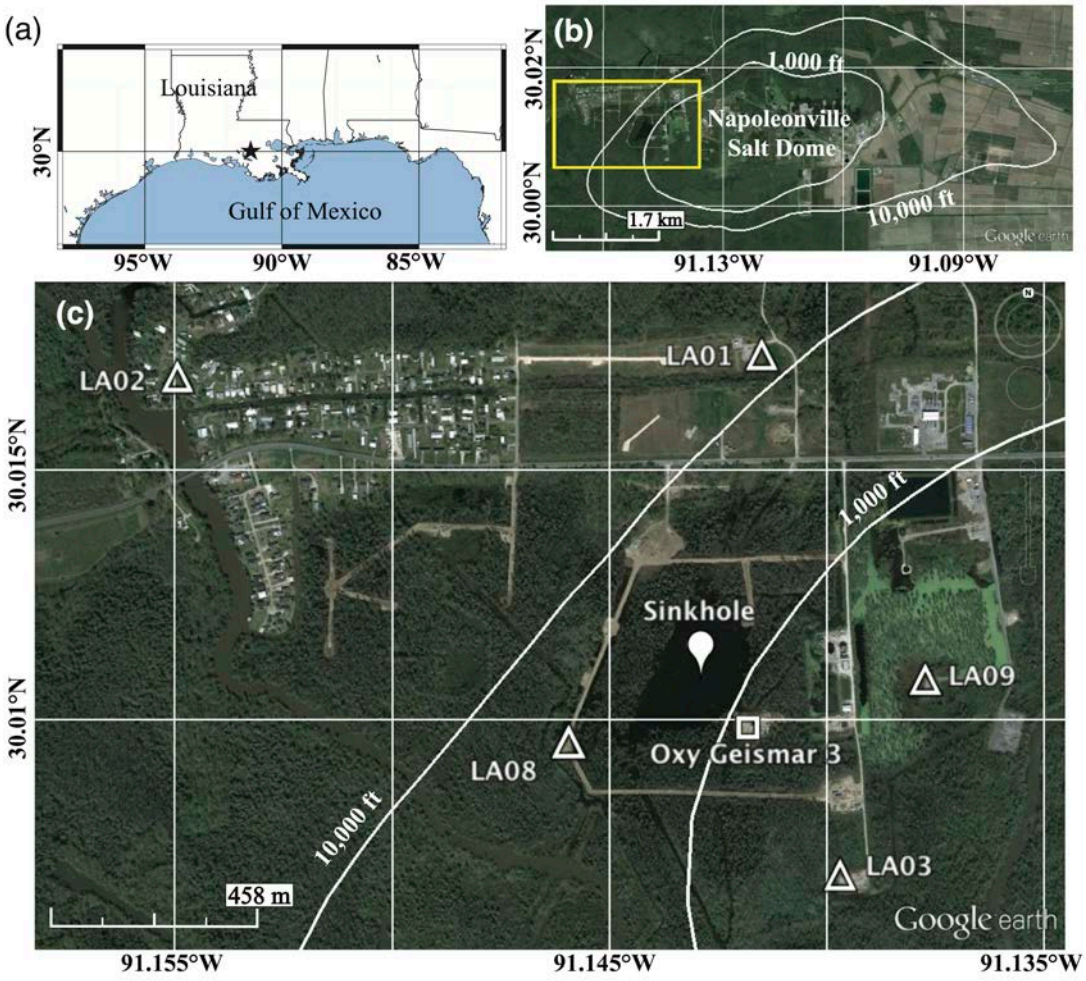

Figure 21. (a) Location of the study region (black star) relative to the state of Louisiana (southeastern *USA*). Google Earth Images (dated 12 March 2013) show- (b) the study region, indicated by the rectangle and expanded in (c), at the western edge of *NSD* (1000 ft and 10,000 ft contours indicated by white lines; William Ellsworth, *personal comm.*, 2012); (c) Locations of the 5 *USGS* broadband stations used for waveform inversion (white triangles), approximate location of *Oxy Geismar* 3 cavern (white square) and an average point location of the sinkhole (white balloon).

Historical seismicity in the state of Louisiana includes a widely felt magnitude 4.2 earthquake (peak intensity *VI* on *MMI* scale) on 19 October 1930 near Napoleonville, Assumption Parish (Stover and Coffman, 1993), whose epicenter might have been close to the present location of the sinkhole. However, this region (-91.16°E to -91.13°E, 30 °N to 30.025 °N) has experienced little or no seismicity in recent years, with no earthquakes reported in the *National Earthquake Information Center* (*NEIC*) – *Preliminary*

Determination of Epicenters (*PDE*) Bulletin between January 1973 and April 2012. Therefore, the synchronous nature of seismicity and development of the sinkhole suggests that the two phenomena are most likely related. In this study, we investigate source mechanisms of seismic events at the sinkhole, represented by a general 2^{nd} order point source centroid seismic moment tensor (*MT*). We implement a grid search approach, GRiD MT (Kawakatsu, 1998; Tsuruoka *et al.*, 2009) for automatic detection, location and *MT* inversion of these events using available seismic wave velocity models for this area. We show results for the time period of one day just prior to formation of the sinkhole. We check the stability and reliability of the *MT* solutions and interpret them in terms of possible physical processes.

Data and Moment Tensor Inversion

Three-component waveforms were continuously recorded at 40 samples per second by a temporary *USGS* network consisting of Trillium Compact broadband seismometers and a Reftek RT130 digitizer (Figure 21c), which enables the study of this seismic sequence in great detail. We examine events starting from 19:00 hours, 01 August 2012 (just after station *LA09* became operational). As signals at station *LA06* (not shown in Figure 21c, but located *SEE* of sinkhole, at -91.12858 °E, 30.00771 °N) are very weak and have higher noise levels, we haven't used its data in the waveform inversion. Figure 22a shows the 5-hour (19:00 – 24:00 hours, 01 August 2012) 3-component raw seismograms at station *LA02*. A cursory examination shows more than 30 small and large events spanning one order in peak amplitude.

Three component velocity waveforms at station *LA08* for two of these events are shown in Figure 23. The records primarily show strong surface waves. Our analysis of multiple events indicates that the waveforms are quite similar to each other indicating closely spaced hypocenters and a repetitive source process. For most events the duration of strongest ground motions is limited to 5-15 seconds.

Variations in the seismic properties of the subsurface along the specific paths are evident from different characteristics of the broadband, ~ 0.1 to 15 Hz, vertical component velocity waveforms (Figure 24). Stations *LA08*, *LA01* and *LA02* are on sedimentary deposits surrounding the salt dome and show waveforms which are very similar to each other, but quite different from waveforms at stations *LA09* and *LA03* which are on sediments over the salt dome. This suggests that the salt dome structure affects seismic wave propagation over these relatively short source-receiver distances.

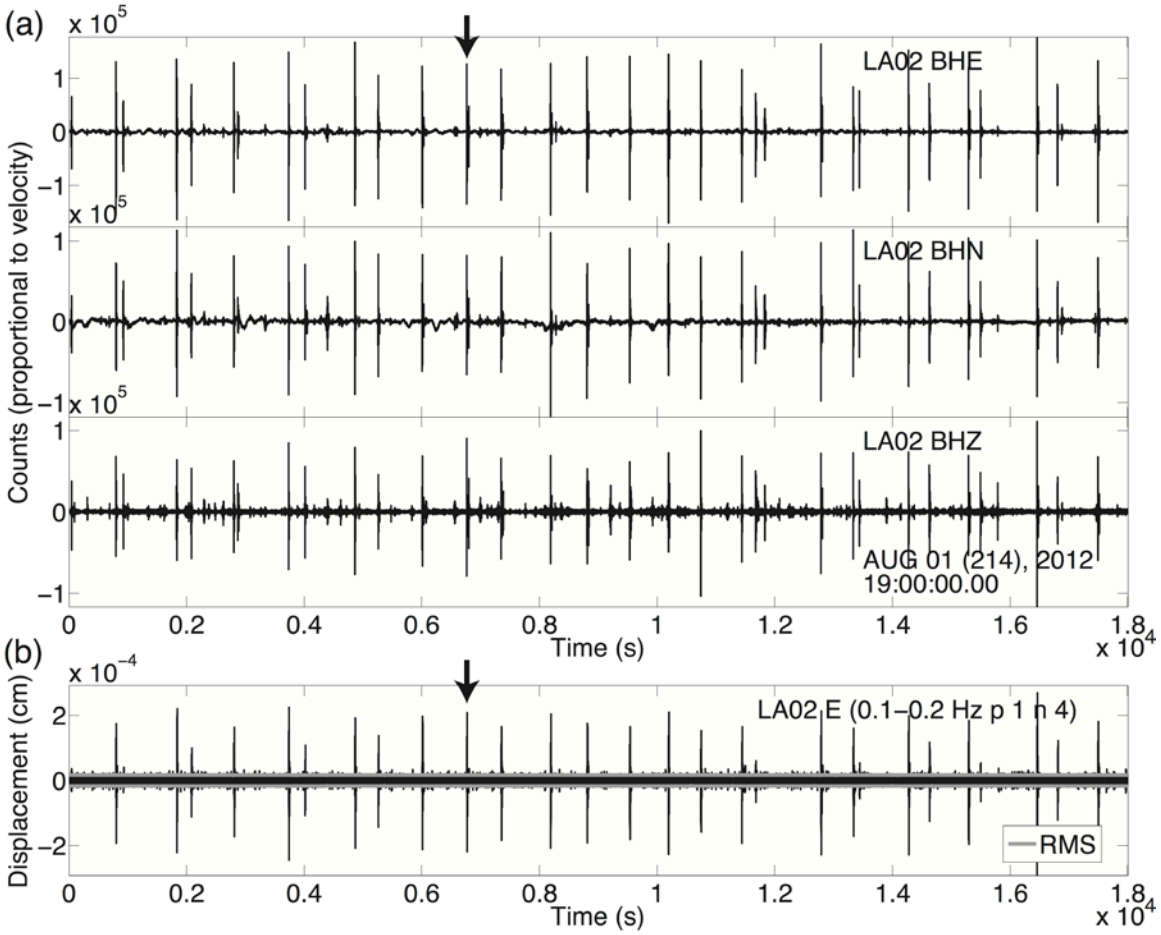

Figure 22. (**a**) Raw 5-hour record on 01 August 2012 at station *LA02. The arrow at the top points to the event TE1 analyzed in detail in the following sections.*
Figure 22. (**b**) E-W displacement at *LA02* in the frequency range used in this study for the same time period as (a). *Gray lines indicate the overall background signal level (±RMS) where RMS (Root Mean Square) = 1.76x10^{-5} cm.*

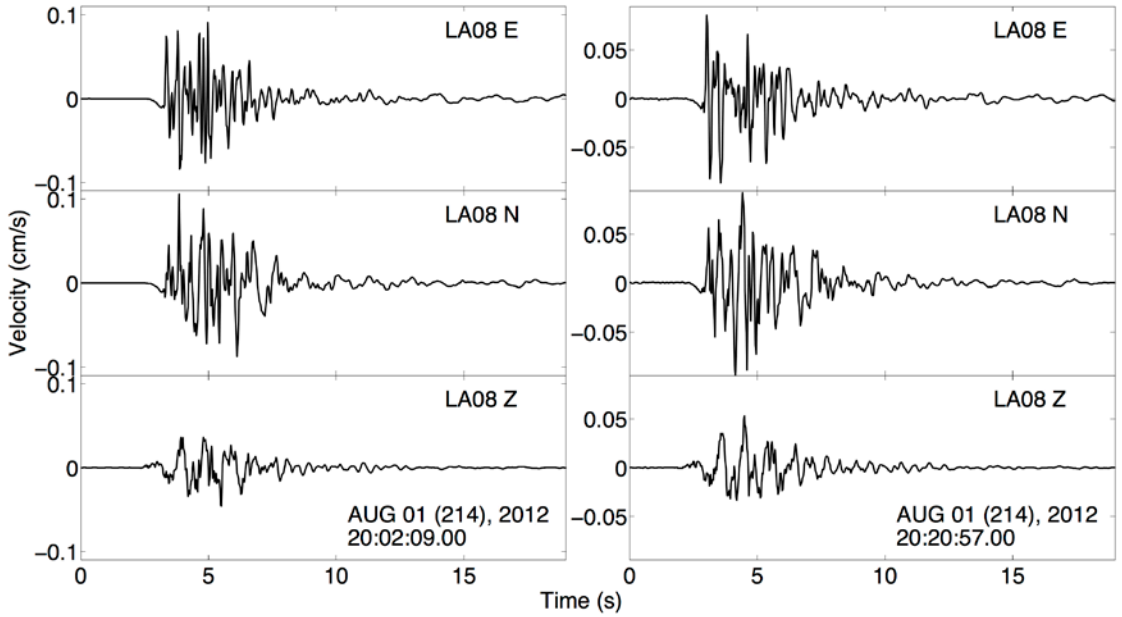

23. Velocity waveforms for two different events at station *LA08*.

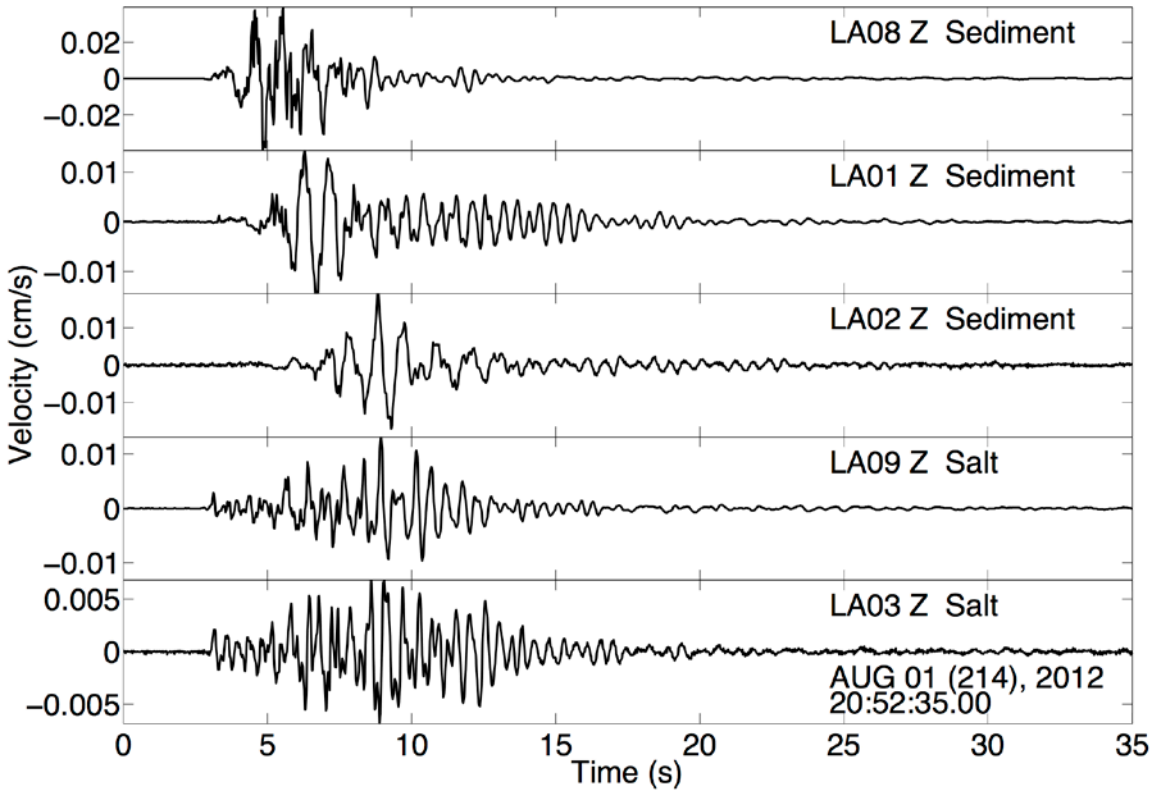

Figure 24. Vertical component velocity records for one event (*TE1*) at all five stations.

The time-independent, 2nd order, 6-component general *MT* (Jost and Herrmann, 1989; Minson and Dreger, 2008) is routinely used to describe the source mechanisms of seismic events. The scalar seismic moment and therefore the M_W are determined, and the *MT* describes the mechanism in terms of body force equivalents, i.e., double couples and linear vector dipoles, assuming a point source in space and time. It can be decomposed into isotropic (volume change) and deviatoric (zero volume change) components. Typically earthquakes are adequately described by a double-couple (*DC*) mechanism in which one of the eigenvalues is zero and the other two are equal and opposite in sign, although small non-double-couple solutions are often found due to noise in the data, unaccounted path effects (Panning *et al.,* 2001), or possible complications in the source process involving non-planar rupture (Julian *et al.*, 1998). The *MT* also enables the study of seismic source processes for non-earthquake events such as nuclear explosions (Ford *et al.*, 2009a, b) and mine collapses (Ford *et al.,* 2008) that involve volume changes that result in significant isotropic components (*ISO*) in their *MT* solutions. The *MT* inversion methodology is described in detail in Jost and Herrmann (1989), Julian *et al.* (1998), and Minson and Dreger (2008). Requirements of a standard *MT* inversion are a hypocenter and a sufficiently accurate velocity model. The inversion then solves for the *MT* and the source depth. The emergent nature of first arrivals in waveforms of the seismic events at the Louisiana sinkhole (i.e., in Figures 23 and 24) makes accurate picking of *P*-wave and *S*-wave arrivals difficult. Moreover, given that the distances are very small, a small uncertainty in arrival times will translate to a large relative error in event location. The available 1D velocity models (Figure 25) of the study region (William Ellsworth, *personal comm.*, 2012) show large differences between seismic wave velocities at the salt dome and surrounding sedimentary structure, which is in turn reflected in the broadband seismic waveforms as already explained in Figure 24. The sediment velocity model shows smoothly increasing velocities with gradients decreasing with increasing depth. The velocity model over the salt dome consists of steep velocity gradients associated with sediments over the salt dome up to a depth of ~250 m. The salt dome is considered to be a fast half space with V_P = 4.5 km/s and V_S = 2.5 km/s, surrounded and overlain by slower sedimentary layers. The 3D nature of the subsurface is bound to influence estimates of the source location and *MT* solution at shorter periods, however considering two 1D velocity models as a first approximation is a reasonable approach if long-period data are used. The *P*-wave and *S*-wave first arrival times computed using these velocity models and the ray-tracing algorithm of Zhao *et al.* (1992) are found to be weakly sensitive to depth, leading to large uncertainties in depth estimates. Moreover, the large number of seismic events, more than 100 on some days, makes a standard event-by-event analysis of location and *MT* impractical.

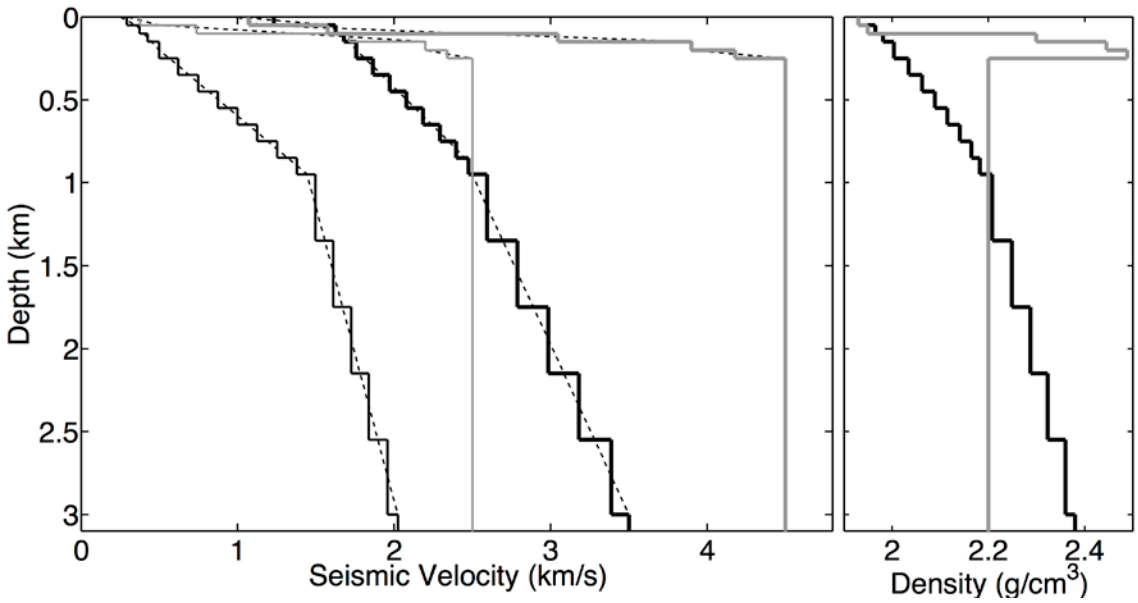

Figure 25. Velocity and density models used in this study. *Gray and black lines represent salt and sediment models, respectively. For velocities, thick and thin lines represent V_P and V_S, respectively. The thin dashed black lines are original smooth velocity models with gradients, which were discretized into layers and used to compute GF.*

In light of the above-mentioned difficulties, we employ the grid-search approach, GRiD MT, of Kawakatsu (1998), which continuously scans the seismic wavefield and performs *MT* inversions of relatively low frequency waveforms assuming virtual point sources distributed over a 3D grid. For a given time window of data, the source location and *MT* solution which give the best Variance Reduction (*VR*), a measure of normalized goodness-of-fit between observed and synthetic waveforms (Minson and Dreger, 2008), is inferred to be the true seismic source. This approach has been used for detection and source characterization of offshore earthquakes in Japan using streaming long-period waveforms (Tsuruoka *et al.*, 2009) and has been modified for a tsunami early warning application for megathrust earthquakes (Guilhem and Dreger, 2011; Guilhem *et al.*, 2013). Based on preliminary analyses, we construct a grid extending from 30.007 °N to 30.0136 °N, -91.1452 °E to -91.138 °E and depth 0.02 km to 1.77 km with grid spacing 0.0006° and 50 m in horizontal and vertical directions, respectively. This grid spans the entire present volume extent of the probable source regions, the sinkhole and the *Oxy Geismar* 3 cavern, which extends in depth from ~ 1.0 to 1.7 km (Report 1, 2013). Three component broadband velocity waveforms are first corrected for instrument response and then integrated to displacement. At sufficiently low frequencies the seismic waveforms become less sensitive to small-scale heterogeneities in earth structure making simplified and approximate velocity models applicable, and the seismic source can be treated as an effective point source in space and time. We have tried a range of filters with different corner frequencies and pole-orders and found that a causal 4-pole Butterworth bandpass filter with corner frequencies at 0.1 Hz and 0.2 Hz greatly simplifies the displacement waveforms while clearly distinguishing signals of larger events from the noise floor (Figure 22b); this filter is subsequently applied to both observed and synthetic

waveforms. It is also important to note that there is a narrowband weakly damped harmonic signal at 0.4 Hz in many of the events that precludes using shorter periods, but which may be indicative of a triggered acoustic wave phenomena within the brine filled cavity, or resonance possibly induced by unsteady fluid flow through a tensile crack (Chouet, 1986; Kumagai *et al.*, 2002). Detailed analysis and modeling of this harmonic signal is beyond the scope of this paper, which focuses on the *MT* analysis, and will be investigated in future work.

For waveform modeling in subsequent sections, seismic paths to stations *LA01*, *LA02* and *LA08* are assumed to conform to the sediment velocity model and seismic paths to stations *LA03* and *LA09* are assumed to conform to the salt dome velocity model. For V_P > 1.5 km/s, density values for sedimentary layers are computed from V_P values using Gardener's rule, $\rho = 1.74\ V_P^{0.25}$ (Gardener *et al.*, 1974). For V_P < 1.5 km/s, density is kept constant at 1.93 g/cm^3. Salt density is assumed to be 2.2 g/cm^3. At such small distances (< 2.0 km), which are smaller or comparable to seismic wavelengths being used, waveforms are expected to be weakly affected by anelastic attenuation. Therefore, regional Q_P and Q_S values are assumed to be 200 and 100, respectively. The effects of different values of *Q* on synthetic waveforms were analyzed afterwards and displacement amplitudes at these low frequencies were found to be insensitive to Q_S values down to 25, with $Q_P = 2 \times Q_S$. The smoothly varying 1D sediment and salt dome velocity models were discretized to layered models and Greens' functions (*GF*) were computed for all grid point depths and all distances from 0.01 km to 2.15 km with precision of 0.01 km using the frequency-wavenumber integration software *FKRPROG* developed by C.K. Saikia based on the methods of Haskell (1964), Dunkin (1965), Watson (1970), Wang and Herrmann (1980) and Saikia (1994). *GF* are filtered in the same way as data and decimated to 0.5 seconds sampling. A 25 second time window is extracted from filtered data and then decimated to 0.5 seconds. Assuming each grid point as a virtual source, a full 6-component (M_{XX}, M_{YY}, M_{ZZ}, M_{XY}, M_{YZ}, M_{ZX}) *MT* inversion is performed using expressions from Minson and Dreger (2008). The *VR* is calculated for each inversion and is used to assess goodness-of-fit and to identify the best fitting solution. The time shift to select the next time window is 0.25, 0.5 or 1.0 seconds depending on the value of best *VR* from previous time window (< 35% or between 35% and 55% or > 55%, respectively). This ensures that the grid search traverses noise windows faster, which typically return poor values of *VR*, while maintaining the origin time resolution at 0.25 seconds. Coarse sampling of waveforms and adaptive time shifting make the algorithm computationally fast.

GRiD MT is applied to data shown in Figure 22. The results, in the form of the change in *VR* with time, are shown in Figure 26. After assuming a threshold *VR* of 70%, which is well above the mean background *VR*, we find 23 events during this period. We have also detected some other unusual signals, both long period and tremor-like, which are usually restricted to the closer stations (*LA03*, *LA08* and *LA09*) and might be related to tilts or some near-field deformation in the source region, unsteady fluid flow, or local noise sources (signals not correlated across multiple stations). Since broadband characteristics of these signals are completely different from signals of the discrete seismic events we are focusing on, they are not included in this study. Details of the *MT* solution and corresponding waveform fits for the best event in this time period, event

TE1 (indicated in Figures 22 and 26) are shown in Figure 27a. This event was located at grid point -91.1422 °E, 30.0112 °N, depth 0.47 km and centroid time 01 August 2012, 20:52:39.00 hours. The solution fits the data very well at *VR* 84.8% and can explain most of the strong radial and vertical components. We find a large volume increase component (*ISO* 72%) in the full *MT* solution. Following the definition of Bowers and Hudson (1999), the scalar Seismic Moment (M_0) of the events is calculated as, $M_0 = M_I + M_D$, where $M_I = |(m_1 + m_2 + m_3)/3|$ is the isotropic moment, $M_D = \max(|m_j - (m_1 + m_2 + m_3)/3|)$ is the deviatoric moment, and m_1, m_2 and m_3 are the eigenvalues of a general moment tensor *M*. Event *TE1* has a scalar moment thus defined of 2.4e+18 dyne.cm, corresponding to a M_W 1.53. The spatial distribution of *VR* in Figures 27b and 27c shows that our centroid location is fairly well constrained, and located east of the sinkhole, at the edge of the salt dome. Despite the long seismic wavelengths, the use of three-component complete waveforms provides both arrival time and azimuth dependent polarity information for various phases, thereby strongly constraining the locations. We suspect that these events are occurring within the salt, but at this point, we are unable to precisely put the event in the salt or the surrounding sediments due to the coarse grid spacing (~ 60 m), the large seismic wavelengths of data used in the inversion, and the uncertainties in 3D geometry of the salt dome and seismic velocity structure.

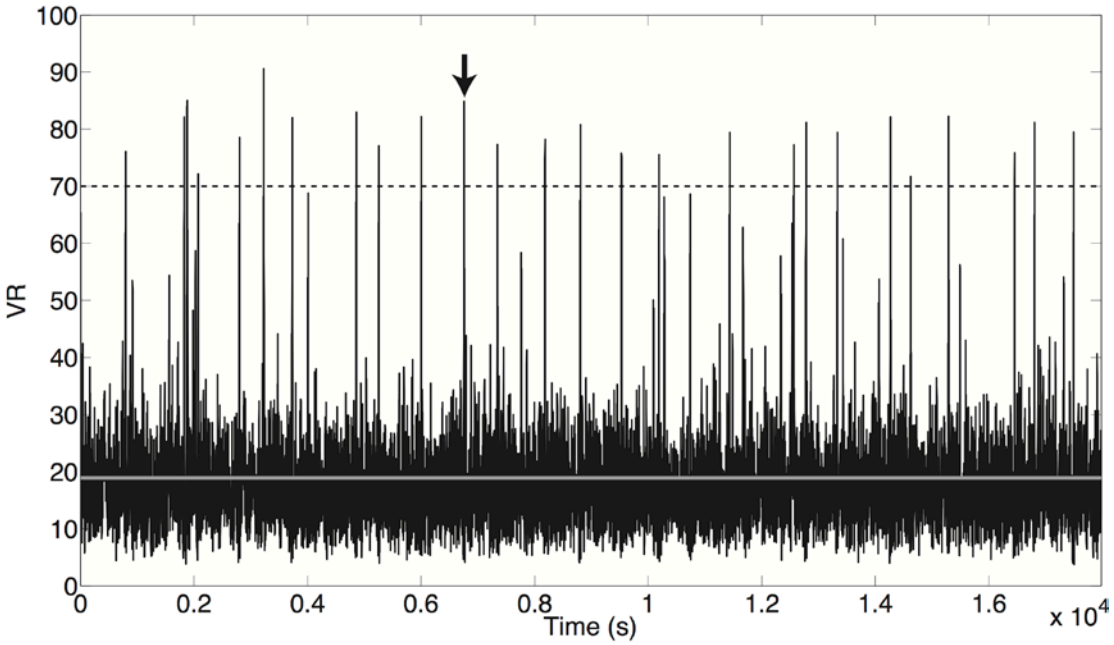

Figure 26. Plot of *VR* with time for data shown in Figure 22. *Peaks with VR > 70% (dashed line) are considered to be probable seismic events. The arrow at the top points to event TE1 indicated in Figure 22. The gray line indicates the mean background VR (18.9 %) for this time period.*

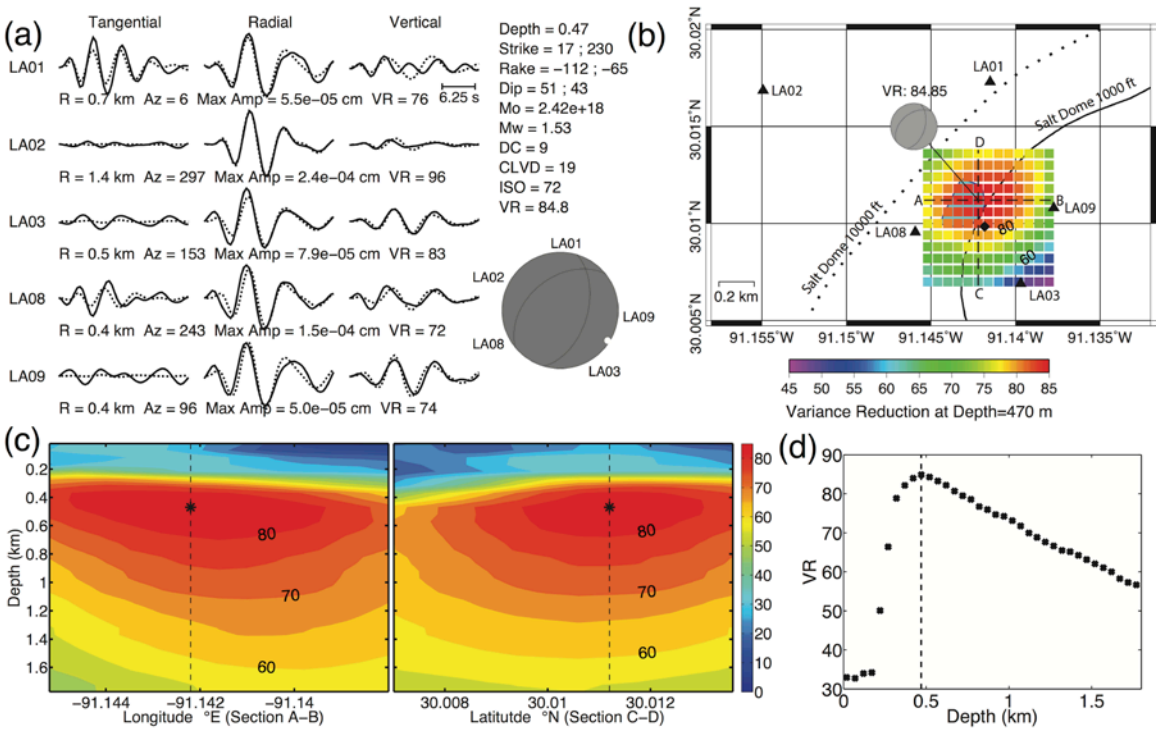

Figure 27. (**a**) Observed (solid lines) and synthetic (dashed lines) 0.1-0.2 Hz displacement waveforms and full *MT* solution for event *TE1*; *R* = epicentral distance, az = azimuth (°), Max Amp = maximum displacement amplitude at a station.
Figure 27. (**b**) Grid-search results for full *MT* solution of event *TE1* shown in (a). *Squares show VR at grid points at 470 m depth. Solid and dotted lines are 1,000 ft and 10,000 ft depth contours of NSD. Depth sections of VR across profiles A-B and C-D (dashed lines) through the best fitting centroid location are shown in (c). Shaded polygon (below the grid) = approximate surface extent of the sinkhole in July 2013; black triangles = station locations; black diamond = Oxy Geismar 3 cavern.*
Figure 27. (**c**) Depth sections across profiles *A-B* and *C-D* showing smoothed variations of *VR*. *Black star is the best-fitting centroid hypocenter of event TE1 and the thin dashed line is the line of intersection of the two sections.*
Figure 27. (**d**) Values of best *VR* at various grid point depths.

Figure 28 shows the spatial distribution of *MT* solutions represented by *P*-wave first motion mechanisms for all 23 events detected during the time period of Figure 22. Reflecting the similarity in waveforms, mechanisms for all events are very similar to each other. The events are approximately concentrated at the western edge of the salt dome, very close to the sinkhole. We have also analyzed the data of 02 August 2012 up to 19:00 hours. We observe a drop in seismicity after 02 August 2012 corresponding to the day when the sinkhole was first discovered. Overall, the mechanisms and locations are very similar to those shown in Figure 28.

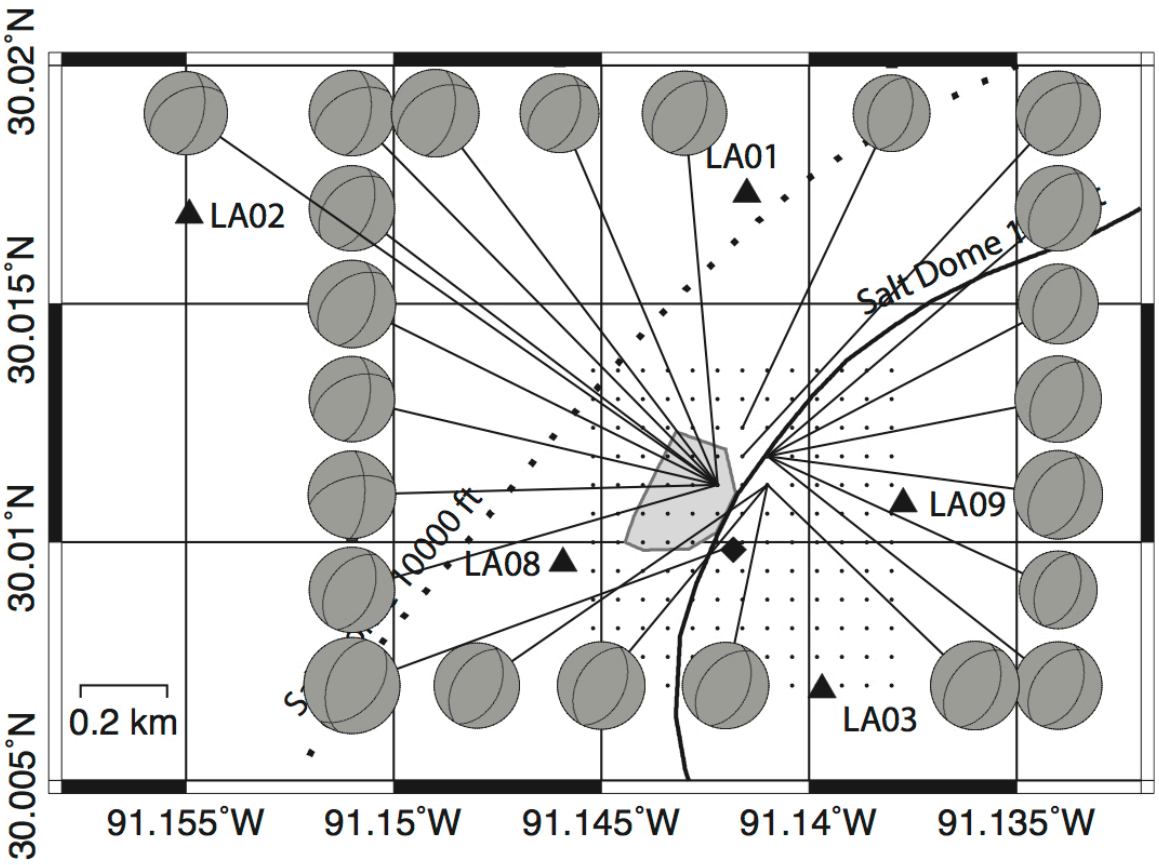

Figure 28. Mechanisms and locations of the events detected in the time period shown in Figure 22. *Meaning of other symbols is same as in Figure 27b.*

The *MT* solutions show a dominant volume increase component, which is quite the opposite to what one would expect in a collapse environment, if the energy release were purely due to gravity driven collapse alone (Ford *et al.*, 2008). We calculate the two *MT* source-type parameters, ε and k, for all events and plot them on the Hudson source-type plot (Hudson *et al.*, 1989) shown in Figure 30. The horizontal axis plots the ratio of the deviatoric eigenvalues, ε, and the vertical axis plots k, the relative isotropic component. *MT* solutions for the Louisiana sinkhole seismic sequence plot somewhere close to tensile cracks and explosions, quite far away from natural double-couple earthquakes and expected implosions or closing cracks. Decomposition of full *MT* solutions of these events returns 6-32 % *DC* and 0-27 % *CLVD* components in addition to the spherical tensile source. While the *DC* components are very small, the corresponding fault plane solutions are remarkably similar for all events, indicating that the small deviatoric components in the full *MT* solutions are not random and are possibly due systematic source or path effects. The two mean fault planes (along with standard deviations) consistent with the *DC* components of the *MT* solutions are (Strike 229°±19°, Rake -65°±22°, Dip 47°±7°) and (Strike 18°±7°, Rake -112°±19°, Dip 53°±9°). Using the hypocenters from the full *MT* GRiD MT results (Figure 27b and 27c), we also perform a grid search of source parameters for a shear-tensile (crack+*DC*) *MT* solution for event *TE1* (Minson *et al.*, 2007). A shear-tensile source mechanism combines tensile opening

with shear slip along a single fault plane (Minson *et al.*, 2007; Šílený *et al.*, 2009). Assuming a Poisson's ratio (v) of 0.39 for a source in sediments, we obtain shear-tensile seismic scalar moments, $M_{0,CRACK}$ = 1.71e+18 dyne.cm and $M_{0,DC}$ = 3.7e+17 dyne.cm on fault planes (Strike 225°, Rake -58°, Dip 67°) or (Strike 23°, Rake -120°, Dip 76°), which fit the waveforms well, at almost the same *VR* (~ 84.8 %) as the full *MT* solution. A source in salt (v = 0.28) yields a solution that fits the waveforms poorly at *VR* ~ 78.4 %. This is also reflected in the Hudson plot in Figure 29, where the sinkhole events plot much closer to a theoretical tensile crack in sediments (v = 0.39) than to one in salt (v = 0.28). Keeping the hypocenter fixed, a pure crack in sediments (v = 0.39) also yields good waveform fits at *VR* = 83.1 % whereas a pure isotropic explosion and a pure *DC* source fit the waveforms poorly at *VR* 38.5 % and 60.2 %, respectively.

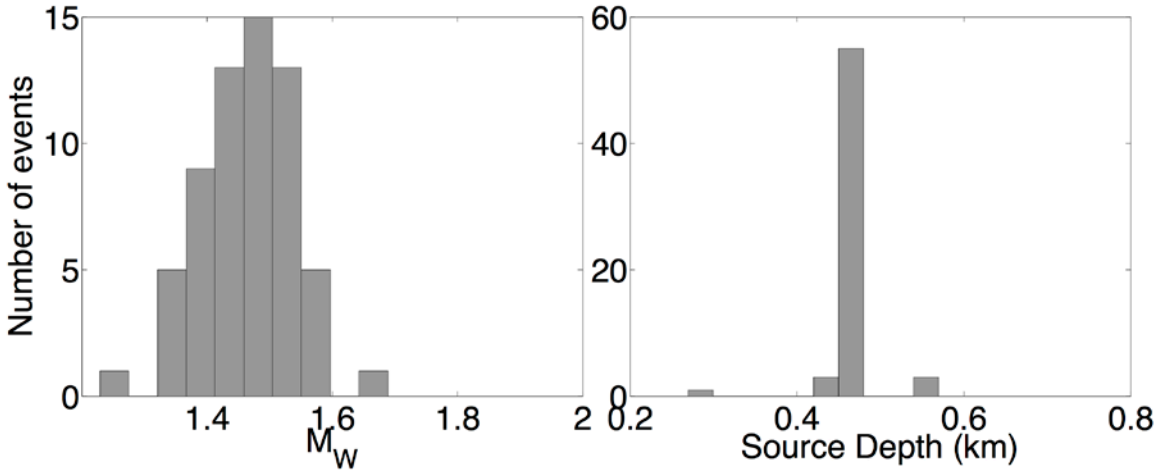

Figure 29. M_W and source depth distribution of all 62 events detected with *VR* > 70%.

To assess confidence in the source mechanisms thus obtained, we compute the Network Sensitivity Solution (*NSS*) (Ford *et al.*, 2010) for event *TE1*. The *NSS* compares fits between observed and synthetic waveforms for a large population ($3x10^7$) of source-types, uniformly distributed moment tensors that generates a distribution of goodness-of-fit in source-type space that allows one to identify the uniqueness of the source-type, and the existence of possible tradeoffs as is common in nuclear explosions (Ford *et al.*, 2010). For each coordinate on the Hudson source-type plot (ε, k), the best *VR* value from all *MT* solutions corresponding to that coordinate is selected, and normalized with respect to the maximum *VR* from the entire space (Figure 30a). It is observed that *MT* solutions that produce best fits (> 95%) are clustered tightly in a region between theoretical explosions and tensile cracks, quite far away from theoretical deviatoric mechanisms, which produce fits only up to 70-75 % of the best possible *VR*. To estimate uncertainties in *MT* solution of event *TE1*, we compute 10,000 full *MT* solutions by bootstrapping residuals from waveform fits for the best fitting full *MT* solution at the same location and depth (Ford *et al.*, 2009a, b). The bootstrapped residuals are first filtered using the same filter applied to waveforms and are then rescaled so that their peak amplitude is equal to the peak amplitude of the original residuals. The 99% confidence ellipse of distribution of these solutions in Hudson space is shown in Figure 31a. The distributions of *MT* elements and *DC*, *CLVD* and *ISO* components for these solutions are shown in Figure 31b. The standard deviations of normal-like distributions of the *MT* elements represent the

uncertainties in the *MT* solution. The uncertainties in the larger *MT* elements, M_{XX}, M_{YY} and M_{ZZ}, are of the order of ~ 2e+17 to 4e+17 dyne.cm which is ~ 9 to 30 % of their absolute values (1.3e+18 to 2.1e+18 dyne.cm). While the uncertainties in the smaller *MT* elements, M_{XY}, M_{YZ} and M_{ZX}, are large, about 30%, 50% and 1000% of the absolute values, respectively, their absolute values and maximum range considering 2 standard deviations are smaller than the absolute values of M_{XX}, M_{YY} and M_{ZZ} by an order of magnitude, thereby strongly constraining the mean *ISO* component to ~ 70% with a small uncertainty (± 4%). The uncertainty in M_{XY}, M_{YZ} and M_{ZX} makes discerning between a vertical tensile crack vs shear-tensile failure uncertain. The shape of the 99% confidence ellipse estimated by bootstrapping waveform residuals closely follows the shape of the 98% contour of best-fitting source-types in the *NSS*, indicating an overall consistency in these estimates.

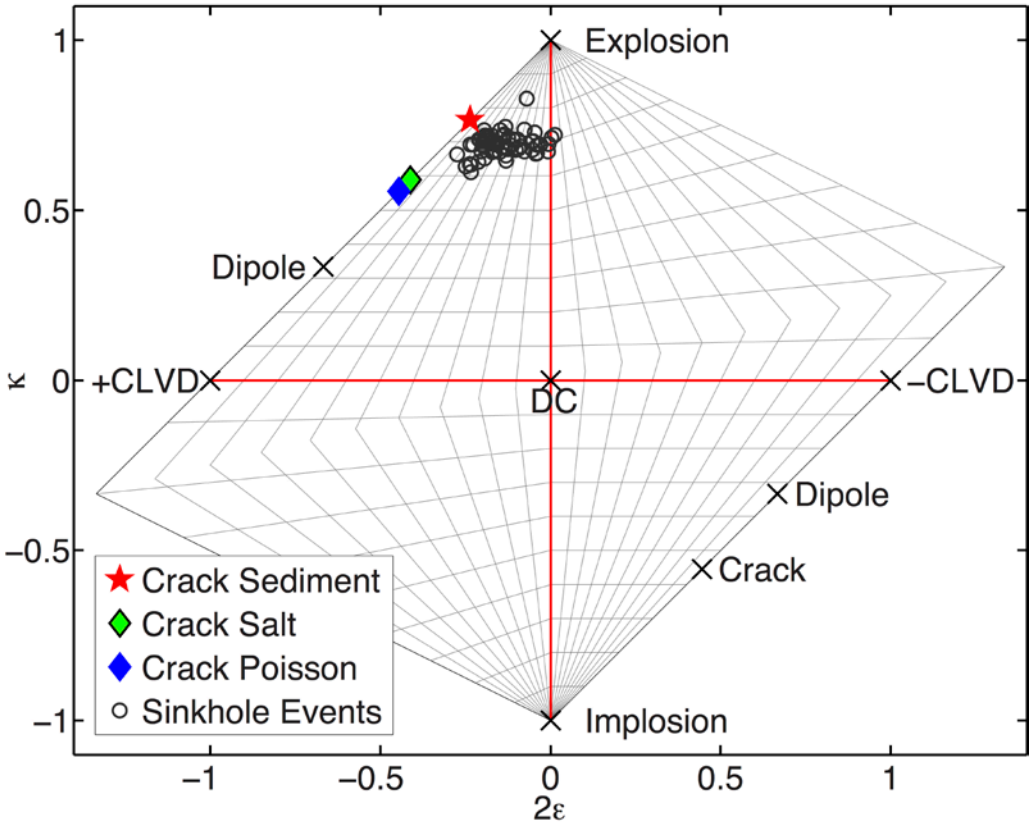

Figure 30. Hudson source-type plot showing major theoretical seismic source mechanisms (black crosses), tensile cracks in various media and 62 events of the Louisiana sinkhole seismic sequence.

For shallow events, Ford *et al.* (2009b; 2010; 2012) observed that *CLVD* sources with vertical axis in compression provided similar quality of fits to explosion waveforms due to their mimicking of explosion source radiation pattern near the equator of the focal sphere which is the region usually sampled by shallow source intermediate-period waveforms. In this case we do not see the same sort of tradeoff in the *NSS* since the near

vertical tensile crack with a primarily horizontal major vector dipole produces strong azimuthal variation in amplitudes, which is not produced by explosions or vertical *CLVD* sources.

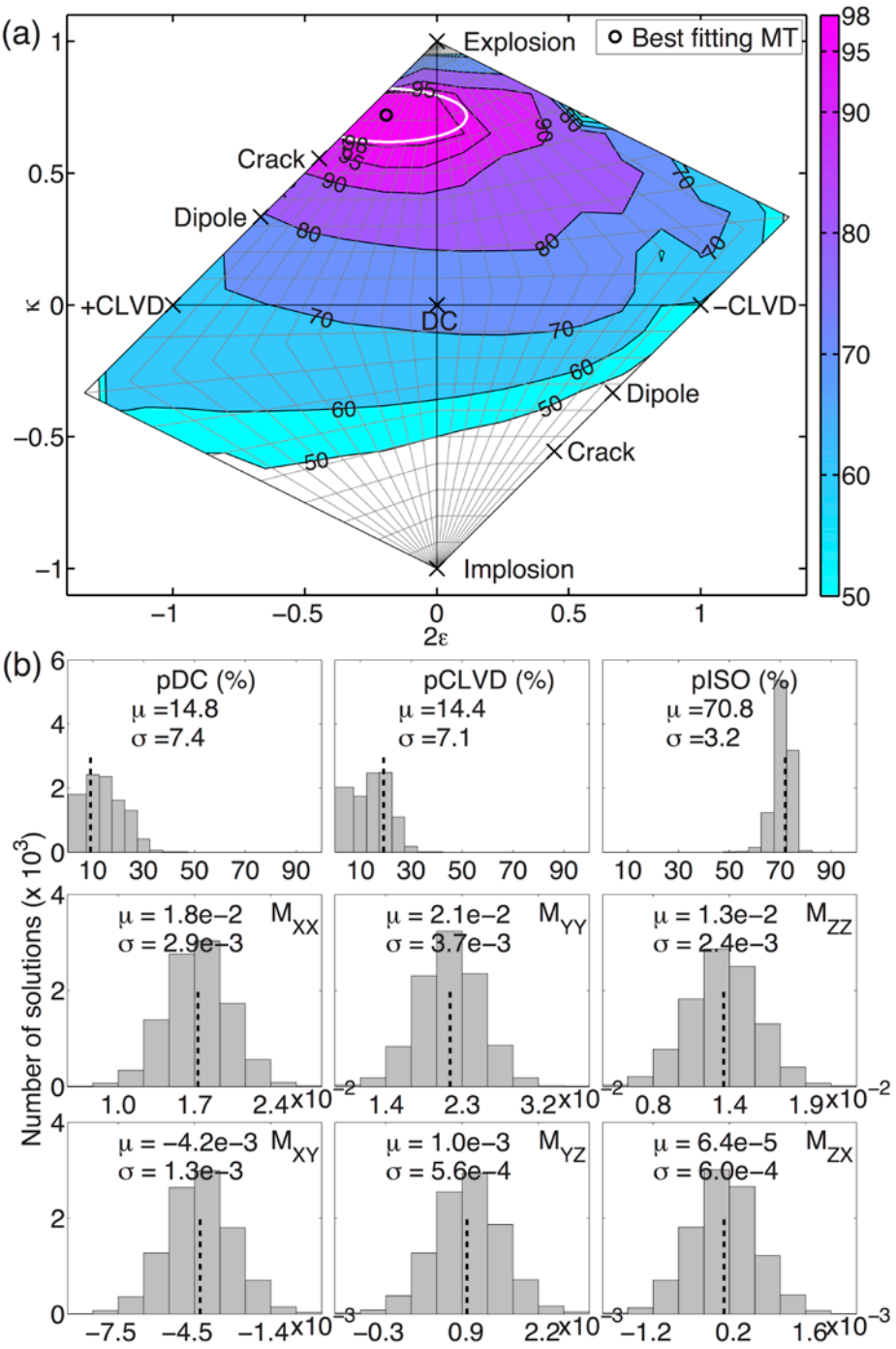

Figure 31. (**a**) Network Sensitivity Solution for event *TE1* using waveforms only. *The white polygon is the 99% confidence ellipse of the distribution of MT solutions computed by bootstrapping residuals.*

Figure 31. (**b**) Distribution of *DC*, *CLVD* and *ISO* components and *MT* elements (units are 1e+20 dyne.cm) from the bootstrap uncertainty analysis of event *TE1*. *The dashed lines represent values corresponding to the best fitting full MT solution.*

Results

In this section, we have implemented a procedure for independent continuous detection, location and *MT* inversion of seismic events at the sinkhole at *NSD*, Louisiana. The computational efficiency and simplicity of the approach makes it suitable for real-time applications or analyzing large volumes of micro-seismic data in reservoir and mine settings, especially if events are numerous or one is not confident in hypocenter estimates based on travel-times alone, as well as for monitoring for possible explosive events in targeted regions. The method has the advantage that given a reasonably calibrated velocity model, and use of relatively long period waves (actual period depends on distances involved), that it is autonomous providing independent event detections, locations, source parameter estimation, and when considering full moment tensor implementations source type discrimination capability. This work has been published in the Bulletin of the Seismological Society of America (Nayak and Dreger, 2014).

3.5. Full MT Analysis of the Berkeley Moment Tensor Catalog and Demonstration of a Statistical Discrimination Basis

A question the current research addresses is whether source-type populations remain separated in other regions of the world, as is the case for NTS and western US seismicity. We have compiled a database of naturally occurring, and induced seismicity to examine the distribution of non-double-couple seismic moment tensors in a Hudson source-type diagram. This database is to be used as an a priori constraint on the complementary probability distribution of an explosion. In addition, we have computed full moment tensor solutions for 877 events in the Berkeley Seismological Laboratory catalog (Figure 32a). These solutions have all been reviewed and are of the highest quality. The mean is $2\varepsilon=0.00544$ and $\kappa=-0.03499$, essentially a double-couple, and the data is normally distributed to first order. The results show that the explosion and large positive CLVD area of the source-type diagram, typical for explosions, is a low probability region for natural seismicity. We have evaluated the significance of improved fit of full moment tensor solutions compared to deviatoric moment tensor solutions for the Berkeley catalog using the F-test. These results indicate that only 20 of the events have statistical significance above 90%, and that the vast majority of events (97.7%) are best characterized as deviatoric without a volumetric term. Of the 20 events with F-test statistical significance above 90% only 7 have statistical significance above 98%. These events occur in the Long Valley Caldera and the Geysers geothermal field where events with large positive volumetric components have been well constrained.

In Figures 33 and 34 we compare the earthquake and explosion data populations to a P-value to test for evidence of explosion. The explosion population included only events from the Ford et al. (2009) study of NTS nuclear explosions. The earthquake population is the BSL catalog shown in Figure 32. For each population a multivariate normal distribution was fit to the data. The distributions were then integrated to find the P-value for the earthquake and explosion null hypotheses. A composite P-value, which is the product of the P-value from the NTS explosion data set, and the complement of the P-value for the BSL full moment tensor earthquake catalog was estimated. The shading on Figures 33 and 34 show the composite P-value. This composite P-value tests for evidence of an event not being an earthquake, and simultaneously for it being an explosion. As Figure 33 shows only a few earthquake events plot in the region of relatively high P-value for explosion evidence, only 6 for P-value>0.5. Thus 6 out of 877 (0.68%) test potentially high as an explosion, however only two of these have F-test significance that would indicate that the isotropic component is resolved. These two events occurred in the Geysers geothermal field where events with isotropic components have been previously observed. Considering a P-value threshold of 0.1 there are 19 out of the 877 events (2% of the events) that misidentify. The majority of these have F-statistics that would indicate the isotropic component of the moment tensor is not statistically significant. The events in this region with F-statistics above 95% (red pluses) are located in the Geysers. Misidentification of earthquakes is a matter for concern. These events also tend to have few stations, and thus the isotropic component is not well resolved, and it is likely that if

independent first motion data were incorporated that the false isotropic component would be eliminated. Examining misidentified earthquakes is the focus of ongoing work.

In Figure 34 the explosion dataset is compared to the composite P-value test. The green plusses are the NTS events used to determine the source type distributions for the P-value analysis, and the red plusses are test events that include the 1988 Soviet JVE, 1995 and 1996 Lop Nor, 1998 India, 2006 and 2009 DPRK nuclear tests, and a forth shallow explosion. All of the events discriminate clearly except for the 1996 Lop Nor (section 3.2) and 1998 India tests. Both of these tests have large F factors indicating reversal of Rayleigh wave polarity. It is noted however that while these two events fail to discriminate clearly given the composite test they are also inconsistent with both explosions and earthquakes. Thus even though explosion discrimination fails for these events they are flagged as unusual requiring additional analysis.

The example provided here is promising in terms of developing a statistical discrimination basis. It makes use of the Hudson et al. (1989) source-type diagram. Recently Tape and Tape (2012) proposed a spherical projection of source-type that is preferred for developing a statistical based discrimination method. Future work will be implementing their projection.

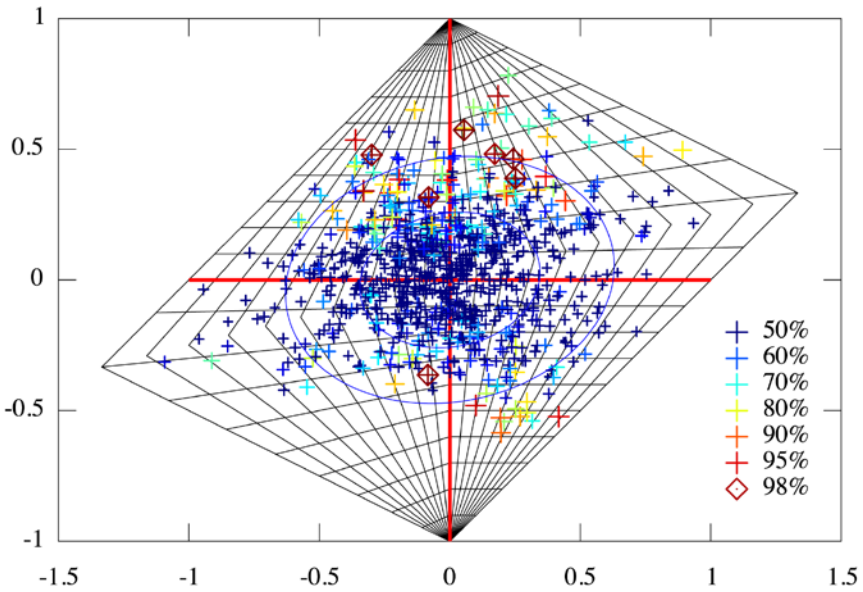

Figure 32. BSL full moment tensor catalog containing 877 events from 1992-2012. *The symbols are color coded to the F-test statistical significance comparing a 5-degree of freedom deviatoric moment tensor solution to the 6-degree of freedom solution that includes the volumetric term. The ellipses show the 50% and 90% population density curves.*

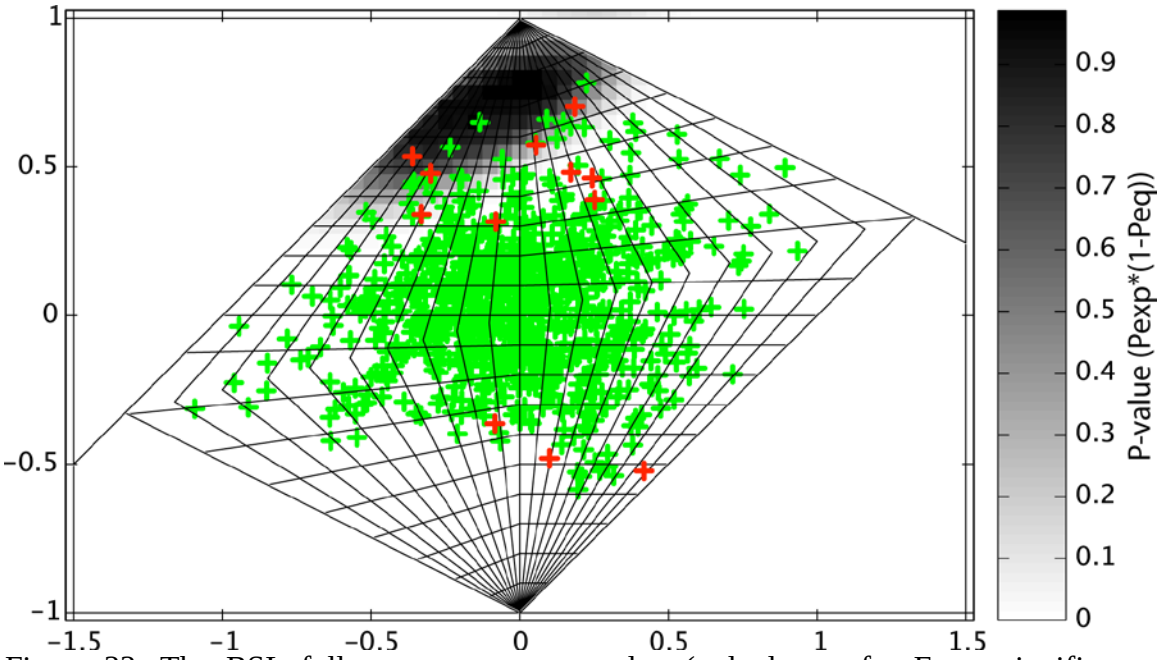

Figure 33. The BSL full moment tensor catalog (red plusses for F-test significance greater than 95%) is compared to the P-value for explosion evidence.

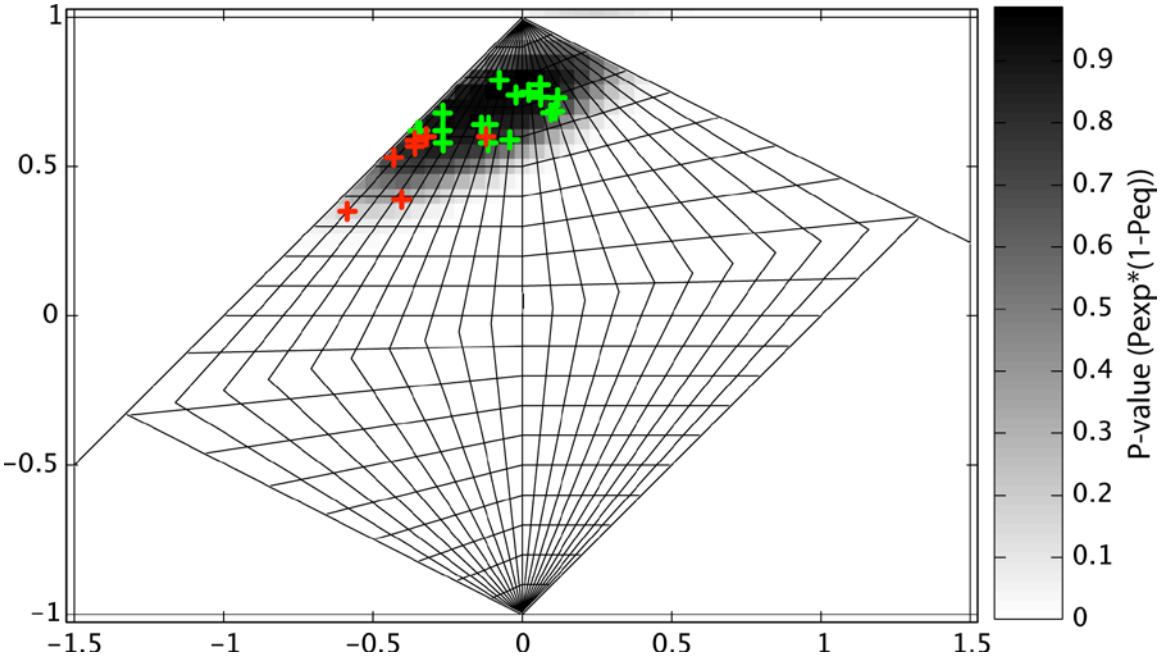

Figure 34. NTS explosions (green plusses), and test explosions (1988 Soviet JVE, 1995 Lop Nor, 1996 Lop Nor, 1998 India 2006 and 2009 DPRK nuclear tests, and a shallow conventional explosion; red plusses) are compared to the composite P-value to test for explosion evidence.

4. RESULTS AND DISCUSSION

The results of this study indicate that a regional distance, complete long-period waveform moment tensor approach is able to uniquely discriminate explosions from earthquakes. The application of this method to the 2009 DPRK event, section 3.1, indicates that the theoretical tradeoff between a pure explosion mechanism and a CLVD mechanism with the major compressional dipole oriented vertically can be eliminated using P-wave first arrival polarities from teleseismic arrays (Figure 2cd). This work was published in Ford et al. (2012). Although polarities provide substantial additional constraint as demonstrated there can be difficulty in reliably picking first P-wave onset for shallow buried sources, and therefore using the teleseismic array beam waveforms is expected to provide stronger constraint. In fact, as Figure 2 shows the forward fit to the array beam P-waveforms is quite good, and it should be possible to incorporate these waveforms in the inverse procedure for determination of the seismic moment tensor.

The results of the study of the 1988 Soviet JVE test, and two nuclear explosions at the Lop Nor test site reveal that a combined long-period waveform and first-motion polarity moment tensor inversion is able to discriminate these explosions from earthquakes under conditions of very sparse recording geometry (as few as three stations) with stations located at 100s to 1600 km from the source region. The incorporation of regional distance P-wave polarities, at the same stations used for long-period waveform constraints, or if available from teleseismic arrays, greatly improves the resolution of source-type (Figures 6 and 7) even for cases in which the tectonic release may be strong enough to reverse polarity of the Rayleigh wave.

Synthetic testing indicates that the vertical dip-slip Green's functions associated with the **M**xz and **M**yz moment tensor components are affected by the vanishing traction at the free-surface in the period range we are interested, between 10 to 50 seconds period. The amplitudes of the Green's functions decrease systematically, but the waveforms are similar over the targeted depth range for nuclear explosions with little phase distortion. Our results show the degree in which free-surface vanishing traction affects the moment tensor solution depends strongly on the velocity model. Velocity models with a shallow velocity gradient show little to no bias in the isotropic and total scalar seismic moment, for both pure explosion source and composite source mechanisms. Similarly, we can retrieve the correct mechanism for these models using the full moment tensor inversion. One possible explanation is that models with a shallow velocity gradient result in more complicated waveforms with numerous phases more completely sampling the focal sphere, thereby providing more constraint on the moment tensor inversion.

Our studies show that including P-wave first motions in addition to full waveform data can eliminate the common ISO-CLVD tradeoff (e.g. Ford et al., 2012; Chiang et al., 2014) and reduce the uncertainties of sparsely recorded underground explosions with strong Love waves (Chiang et al., 2014). Here we demonstrated that although we cannot uniquely characterize the HUMMING ALBATROSS events as predominantly explosive using only waveform data, the combined waveform and first motion method enables the unique discrimination of these small shallowly buried events. The combined method not

only applies to larger manmade and natural seismic events, but also small magnitude, very shallow explosive sources that are effectively at the free surface. The combined method gives a well-constrained NSS even as we go towards longer periods, where the effects of free-surface vanishing traction are more pronounced. The combination of both low frequency full waveform data and high frequency P-wave polarities greatly enhances the capabilities of the moment tensor source-type discrimination method in cases of sparse station coverage, strong Love waves and free-surface effects due to very shallow source depths.

A continuous waveform scanning algorithm was implemented to study micro-earthquakes associated with the collapse of a salt cavern in Louisiana. This application demonstrated the recovery of stable full moment tensor solutions that show these micro-earthquakes are dominated by volume increase components due to the migration of high pressure gas and fluids for the subsurface. This example shows that analysis of such events can be carried out to low magnitudes (Mw 0.8 to 2.1), and for sources at very shallow depth 450m. In this analysis stations were located between 0.5 to 2 km. While this application was for mining induced seismicity it demonstrates that it is possible to autonomously detect, locate, and estimate seismic moment tensor solutions using streaming seismic waveform data. Thus the approach can operate in a realtime processing stream. It also has an advantage in that if a particular region of interested is well calibrated with 3D velocity models that it would be possible to incorporate 3D Green's functions into the processing stream with no reduction in run time since Green's functions are stored as an in-memory database. Using the principle of reciprocity it would be possible to incorporate path specific Green's functions for each of the virtual sources considered in a given virtual source volume. This approach is being used routinely in Japan to monitor offshore seismicity (Tsuruoka et al., 2009), and we are currently implementing the method for seismic monitoring of the Mendocino Triple Junction region to be used as a tsunami early warning algorithm (Guilhem and Dreger, 2011), and appears to be very well suited for targeted nuclear explosion monitoring.

Using a catalog of earthquakes for northern California, and the NTS nuclear explosion results of Ford et al. (2009a) we have demonstrated a statistically based discrimination metric that utilizes the complement of the P-value for earthquake sources (the hypothesis that events are not earthquake like), and the P-value for the NTS nuclear explosions (the hypothesis that events are explosion like). The result of the composite test was applied to the India, JVE, Lop Nor and DPRK nuclear tests. All events cleanly discriminate except for India and the 1996 Lop Nor tests, which show large Love wave excitation and evidence for reversed polarity Rayleigh waves. In these two cases the events fall in a region that would indicate a suspicious source signature.

5. CONCLUSIONS

This research demonstrates the utility of a regional distance, long-period waveform moment tensor inversion approach for nuclear event discrimination. In section 3.1 it is shown that the combination of long-period regional distance waveforms and teleseismic P-wave polarities from array data may be combined in a manner that results in the unique identification of the 2009 DPRK nuclear test as an explosion. In section 3.2 we further develop this approach and apply it to very sparse monitoring conditions for the 1988 Soviet JVE and 1995/1996 Lop Nor nuclear tests. In these cases it was found that the combination of long-period regional distance waveforms combined with P-wave polarity information from the same stations uniquely discriminate these events even under the extremely poor azimuthal and distance coverage. Additionally, it is demonstrated that for the 1996 large F factor test in which Love waves are larger amplitude than long-period Rayleigh waves, and where the tectonic release is large enough to cause reversal of polarity of the Rayleigh waves the combined data approach coupled with the NSS method (Ford et al., 2012) identifies the event as unusual compared to nearby earthquakes. In section 3.3 the effect of shallow depth of burial and the consequent reduction of Green's function amplitude due to vanishing traction at the free surface does not have a detrimental effect on the recovery of seismic moment tensors for shallow explosions, however this is velocity model dependent. The presence of shallow structure that produces multiple phases that more thoroughly sample the focal sphere appears to diminish the effect of underestimation of explosion scalar moment and moment tensor bias that can be observed in cases with simpler velocity structures used for Green's functions. An application with a shallow quarry blast shows that the combination of long period waveforms and first motions leads to unique discrimination of the event as an explosion. In section 3.4 we demonstrate the application of a continuous scanning algorithm that enables the simultaneous detection, location and estimation of the seismic moment tensor from streaming waveform data. The application in this case was for shallow micro-earthquakes associated with a salt dome cavern collapse, however it shows that the method may be applied to very shallow sources, and can provide a complete monitoring capability for targeted regions provided velocity models and Green's functions are suitably calibrated. In section 3.5 it was demonstrated how seismic moment tensor information may be used to define a statistical decision basis for nuclear event discrimination. The statistical metric used is the combination of the P values for a calibration population of nuclear explosions and the complement of the P value for a calibration population of earthquakes. The combined metric was shown to discriminate a number of nuclear explosions not used in the calibration. Although the 1998 India and 1996 Lop Nor tests fail the discrimination they are identified as suspicious being outside of the distribution of naturally occurring earthquakes.

REFERENCES

Battis, J. C. and J. J. Cipar (1991), Seismic recordings in the Northeastern United States of the Shagan River Nuclear Test of 14 September 1988, PL-TR-91-2001, *Geophysics Directorate of Phillips Laboratory,* Hanscom Air Force Base, MA.

Beckman, J. D. and A. K. Williamson (1990), Salt-dome locations in the Gulf coastal plains, south-central United States, *USGS Water-Resources Investigations Report 90-4060*.

Ben-Zion, Y. and J. -P. Ampuero (2009), Seismic radiation from regions sustaining material damage, *Geophys. J. Int.*, **178**, pp. 1351-1356.

Bowers, D. and J. A. Hudson (1999), Defining the scalar moment of a seismic source with a general moment tensor, *Bull. Seismol. Soc. Am.*, **89**, 5, pp. 1390-1394.

Bowers, D. (1997), The October 30, 1994, seismic disturbance in South Africa: Earthquake or large rock burst?, *J. Geophys. Res.*, 102(B5), 9843-57.

Bowers, D. and W. R. Walter (2002), Discriminating between large mine collapses and explosions using teleseismic *P* waves, *Pure Appl. Geophys.*, 159, 803-30.

Burger, R. W., T. Lay, T. C. Wallace, and L. J. Burdick (1986), Evidence of tectonic release in long-period *S* waves from underground nuclear explosions at the Novaya Zemlya test sites, *Bull. Seismol. Soc. Amer.*, **76**, pp. 733-755.

Chiang, A., D. S. Dreger, S. R. Ford, and W. R. Walter (2014), Source characterization of underground explosions from combined moment tensor and first motion analysis, *Bull. Seism. Soc. Am.*, 104, no. 4, pp. 1587-1600.

Chouet, B. A. (1986), Dynamics of a Fluid-Driven Crack in Three Dimensions by the Finite Difference Method, *J. Geophys. Res.*, **91**, B14, pp. 13,967-13,992.

Clark, R. A. and R. G. Pearce (1988), Identification of multiple underground explosions using the relative amplitude method, *Bull. Seis. Soc. Amer.*, 78(2), 885-97.

Day, S. M., J. T. Cherry, N. Rimer, and J. L. Stevens (1987), Nonlinear model of tectonic release from underground explosions, *Bull. Seismol. Soc. Amer.*, **77**, pp. 996-1016.

Dreger, D. S., S. R. Ford, and W. R. Walter (2008), Source analysis of the Crandall Canyon, Utah, mine collapse, *Science*, **321**, p. 217.

Dunkin, J. W. (1965), Computation of modal solutions in layered, elastic media at high frequencies, *Bull. Seismol. Soc. Am.*, **55**, 2, pp. 335-358.

Ekström, G. and P. G. Richards (1994), Empirical measurements of tectonic moment release in nuclear explosions from teleseismic surface waves and body waves, *Geophys. J. Int.*, **117**, pp. 120-140.

Ellsworth, W. L., S. Horton, H. Benz, B. Chouet, P. Dawson, S. Hickman, A. Leeds, W.S Leith, M. Meremonte, J. L. Rubinstein, D. Shelly, M. M Withers, and R. B. Herrmann (2012), Tremors in the Bayou: The events on the Napoleonville Salt Dome, Louisiana, *AGU Fall Meeting*, 2012.

Ford, S., D. S. Dreger, and W. R. Walter (2008), Source characterization of the August 6, 2007 Crandall Canyon Mine seismic event in Central Utah, *Seismol. Res. Lett.*, **79**, pp. 637-644, doi: 10.1785/gssrl.79.5.637.

Ford, S. R., D. S. Dreger, and W. R. Walter (2009a), Identifying isotropic events using a regional moment tensor inversion, *J. Geophys. Res.*, **114**, B01306, doi:10.1029/2008JB005743.

Ford, S. R., D. S. Dreger, and W. R. Walter (2009b), Source analysis of the Memorial Day Explosion, Kimchaek, North Korea, *Geophys. Res. Lett.*, **36**, 21, L21304, doi:10.1029/2009GL040003.

Ford, S. R., D. S. Dreger, and W. R. Walter (2010), Network sensitivity solutions for regional moment-tensor inversions, *Bull. Seismol. Soc. Am.*, **100**, 5A, pp. 1962-1970, doi: 10.1785/0120090140.

Ford, S. R., W. R. Walter, and D. S. Dreger (2012), Event discrimination using regional moment tensors with teleseismic-P constraints, *Bull. Seismol. Soc. Am.*, **102**, 2, pp. 867-872, doi: 10.1785/0120110227.

Gardner, G. H. F., L. W. Gardner, and A. R. Gregory (1974), Formation velocity and density-the diagnostic basics for stratigraphic traps, *Geophysics,* **39**, pp. 770-780.

Given, J. W. and G. R. Mellman (1986), Estimating explosion and tectonic release source parameters of underground nuclear explosions from Rayleigh and Love wave observations, AFGL-TR- 86-0171(I), Air Force Geophysics Laboratory.

Guilhem, A. and D. S. Dreger (2011), Rapid detection and characterization of large earthquakes using quasi-finite source Green's functions in continuous moment tensor inversion, *Geophys. Res. Lett.*, **38**, L13318, doi:10.1029/2011GL047550.

Guilhem, A., D. S. Dreger, H. Tsuruoka, and H. Kawakatsu (2013), Moment tensors for rapid characterization of megathrust earthquakes: the example of the 2011 M9 Tohoku-oki, Japan earthquake, *Geophys. J. Int.*, **192**(2), pp. 759-772 doi:10.1093/gji/ggs045.

Haskell, N. A. (1964), Radiation pattern of surface waves from point sources in a multi-layered medium, *Bull. Seismol. Soc. Am.*, **54**, 1, pp. 377-393.

Horton, S. P., W. L. Ellsworth, J. L. Rubinstein, and M. Withers (2013), Seismological observations associated with the development of a sinkhole near the Napoleonville Salt Dome, Louisiana, *SSA Annual Meeting*, 2013.

Hudson, J. A., R. G. Pearce, and R. M. Rogers (1989), Source type plot for inversion of the moment tensor, *J. Geophys. Res.*, **94**, B1, pp. 765-774.

Julian, B. R., A. D. Miller, and G. R. Foulger (1998), Non-Double-Couple earthquakes – 1. Theory, *Rev. Geophys.*, **36**, 4, pp. 525-549.

Jost, M. L. and R. B. Herrmann (1989), A student's guide to and review of moment tensors, *Seismol. Res. Lett.*, **60**, 2, pp. 37-57.

Kawakatsu, H. (1998), On the realtime monitoring of the long-period seismic wavefield, *Bull. Earthq. Res. I. Tokyo,* **73**, pp. 267-274.

Kumagai, H., B. A. Chouet, and M. Nakano (2002), Waveform inversion of oscillatory signatures in long-period events beneath volcanoes, *J. Geophys. Res.*, **107**, B11, 2301, doi:10.1029/2001JB001704.

Minson, S. E., D. S. Dreger, R. Burgmann, H. Kanamori, and K. M. Larson (2007), Seismically and geodetically determined non-double couple source mechanisms from the Miyakejima volcanic earthquake swarm, *J. Geophys. Res.*, **112**, B10308, doi:10.1029/2006JB004847.

Minson, S. E. and D. S. Dreger (2008), Stable inversions for complete moment tensor, *Geophys. J. Int.*, **174**, pp. 585-592, doi: 10.1111/j.1365-246X.2008.03797.x.

Nayak, A. and D. S. Dreger (2014), Moment tensor inversion of seismic events associated with the sinkhole at Napoleonville Salt Dome, Louisiana, *Bull. Seism.*

Soc. Am., 104:1763-1776.

Panning, M., D. S. Dreger, and H. Tkalcic (2001), Near-source velocity structure and isotropic moment tensors: a case study of the Long Valley Caldera, *Geophys. Res. Lett.*, **28**, pp. 1815-1818.

Patton, H. J. and S. R. Taylor (2008), Effects of shock-induced tensile failure on m_b-M_S discrimination: Contrasts between historic nuclear explosions and the North Korean test of 9 October 2006, *Geophys. Res. Lett.*, **35**, L14301, doi:10.1029/2008GL034211.

Patton, H. J. and S. R. Taylor (2011), The apparent explosion moment: Inferences of volumetric moment due to source medium damage by underground nuclear explosions, *J. Geophys. Res.*, **116**, B03310, doi:10.1029/2010JB007937.

Pearce, R. G., J. A. Hudson, and A. Douglas (1988), On the use of P-wave seismograms to identify a double-couple source, *Bull. Seis. Soc. Amer.*, 78(2), pp. 651-671.

Priestly, K. F., W. R. Walter, V. Martynov, and M. V. Rozhkov (1990), Regional seismic recordings of the Soviet nuclear explosion of the joint verification experiment, *Geophys. Res. Lett.*, **17**, pp. 179-182.

Rautian, T. G. and V. I. Khalturin (1978), The use of coda for determination of the earthquake source spectrum, *Bull. Seismol. Soc. Am.*, **68**, pp. 923-948.

Report 1 (2013), Blue Ribbon Commission - Initial Technical Briefing, Louisiana State University, 05 April 2013. http://dnr.louisiana.gov/assets/OC/BC_All_Updates/Plans_Reports/BlueRibb.04.05.13.pdf (last accessed August 2013).

Report 2 (2013), Office of Conservation, Louisiana DNR – Bayou Corne- ongoing investigation and response (presentation to the Joint Legislative Committees, Baton Rouge, Louisiana), 19 February 2013. http://dnr.louisiana.gov/assets/OC/BC_All_Updates/DNR.House.Senate.19Feb13.pdf (last accessed August 2013).

Rogers, R. M. and R. G. Pearce (1992), Use of relative amplitude method to compute "best-fit" earthquake moment tensors, *J. Geophys. Res.*, 97(B10), 14083-95.

Saikia, C. K., (1994), Modified frequency-wavenumber algorithm for regional seismograms using Filon's quadrature: modeling Lg waves in eastern North America, *Geophys. J. Int.*, **118**, pp. 142-158.

Šílený, J., D. P. Hill, L. Eisner, and F. H. Cornet (2009), Non-double-couple mechanisms of microearthquakes induced by hydraulic fracturing, *J. Geophys. Res.*, **114**, B08307, doi:10.1029/2008JB005987.

Snoke, J. A. (2009), Traveltime tables for iasp91 and ak135, *Seismol. Res. Lett.*, **80**, pp. 260-262.

Song, X. J., D. V. Helmberger, and L. Zhao (1996), Broad-Band Modelling of Regional Seismograms: the Basin and Range Crustal Structure, *Geophys. J. Int.*, 125, pp. 15-29, doi:10.1111/j.1365-246X.1996.tb06531.

Stover, C. W. and J. L. Coffman (1993), Seismicity of the United States 1568-1989 (Revised), *U.S. Geological Survey Professional Paper 1527*, *United States Government Printing Office, Washington*, pp. 243-244.

Sun, X., X. Song, S. Zheng, Y. Yang, and M. H. Ritzwoller (2010), Three dimensional shear wave velocity structure of the crust and upper mantle beneath China from ambient noise surface wave tomography, *Earthquake. Sci.*, **23**, pp. 449-463.

Tape, W. and C. Tape (2012), A geometric setting for moment tensors, *Geophysical Journal International*, **190**, pp. 476-498.

Thoms, R. L. and R. M. Gehle (2000), A brief history of salt cavern use (keynote paper), in: Geertman, R. M., ed., *Proceedings of 8th World Salt Symposium*, 7-11 May 2000, part 1, Elsevier B. V., pp. 207-214.

Toksöz, M. N. and H. H. Kehrer (1972), Tectonic strain release by underground nuclear explosions and its effect on seismic discrimination, *Geophys. J. Roy. Astron. Soc.*, **31**, pp. 141-161.

Toksöz, M. N., D. G. Harkrider, and A. Ben-Menahem (1965), Determination of source parameters by amplitude equalization of seismic surface waves. 2. Release of tectonic strain by underground nuclear explosions and mechanisms of earthquakes, *J. Geophys. Res.*, **70**, pp. 907-922.

Tsuruoka, H., H. Kawakatsu, and T. Urabe (2009), GRiD MT (grid-based real-time determination of moment tensors) monitoring the long-period seismic wavefield, *Phys. Earth Planet. In.*, **175**, pp. 8-16, doi:10.1016/ j.pepi.2008.02.014.

Waldhauser, F., D. Schaff, P. G. Richards, and W. -Y. Kim (2004), Lop Nor revisited: Underground nuclear explosion locations, 1976–1996, from double-difference analysis of regional and teleseismic data, *Bull. Seismol. Soc. Am.*, **94**, pp. 1879-1889.

Walter, W. R. and C. J. Ammon (1993). Complete regional seismic waveform inversion for crust and upper mantle structure: the September 14, 1988 JVE explosion, Kazakhstan, Eurasia, UCRL-JC-112844.

Walter, W. R. and H. J. Patton (1990), Tectonic release from the Soviet joint verification experiment, *Geophys. Res. Lett.*, **17**, pp. 1517-1520.

Walter, W. R. and A. J. Rodgers (1999), Regional waveform modeling in southwestern Asia; tectonic release from the May 11, 1998 Indian nuclear tests, 94th SSA Annual Meeting, *Seismol. Res. Lett.*, **70**, p. 228.

Walter, W. R., E. Matzel, M. E. Pasyanos, D. B. Harris, R. Gok, and S. R. Ford (2007), Empirical observations of earthquake-explosion discrimination using P/S ratios and implications for the sources of explosion S-waves. In: 29th Monitoring Research Review: Ground-Based Nuclear Explosion Monitoring Technologies. NNSA, LA-UR-07-5613, pp. 684-693.

Wang, C. Y. and R. B. Herrmann (1980), A numerical study of P-, SV- and SH-wave generation in a plane layered medium, *Bull. Seismol. Soc. Am.*, **70**, 4, pp. 1015-1036.

Watson, T. H. (1970), A note on fast computation of Rayleigh wave dispersion in the multi-layered elastic half-space, *Bull. Seismol. Soc. Am.*, **60**, 1, pp. 161-166.

Wessel, P. and W. H. F. Smith (1998), New, improved version of Generic Mapping Tools released, *EOS Trans., AGU* **79**, p. 579.

Yang, X., R. North, C. Romney, and P. G. Richards (2003), Worldwide nuclear explosions, Chap. 84 of *International Handbook of Earthquake and Engineering Seismology*, W. H. K. Lee, H. Kanamori, P. Jennings, and C. Kisslinger (Editors), Pt. B, Academic, New York, pp. 1595-1599.

Zhao, D., A. Hasegawa, and S. Horiuchi (1992), Tomographic imaging of P and S wave velocity structure beneath Northeastern Japan, *J. Geophys. Res.*, **97**, B13, pp. 19909-19928.

DISTRIBUTION LIST

DTIC/OCP
8725 John J. Kingman Rd, Suite 0944
Ft Belvoir, VA 22060-6218 1 cy

AFRL/RVIL
Kirtland AFB, NM 87117-5776 2 cys

Official Record Copy
AFRL/RVBYE/Robert Raistrick 1 cy

This page is intentionally left blank.